The Physical Properties and Effective Temperature Scale of O-type Stars as a Function of Metallicity. I. A Sample of 20 Stars in the Magellanic Clouds[1]

Philip Massey[2]

Lowell Observatory, 1400 W. Mars Hill Road, Flagstaff, AZ 86001; Phil.Massey@lowell.edu

Fabio Bresolin and Rolf P. Kudritzki

Institute for Astronomy, University of Hawaii, 2680 Woodlawn Drive, Honolulu, HI 96822; bresolin@ifa.hawaii.edu,kud@ifa.hawaii.edu

Joachim Puls and A. W. A. Pauldrach

Universitäts-Sternwarte München, Scheinerstrasse 1, 81679, Munich, Germany; uh101aw@usm.uni-muenchen.de,uh10107@usm.uni-muenchen.de

ABSTRACT

We have obtained *HST* and ground-based observations of a sample of 20 O-type stars in the LMC and SMC, including six of the hottest massive stars known (subtypes O2-3) in the R136 cluster. In general, these data include (a) the *HST* UV spectra in order to measure the terminal velocities of the stellar winds, (b) high signal-to-noise, blue-optical data where the primary temperature- and gravity-sensitive photospheric lines are found, and (c) nebular-free Hα profiles, which provide the mass-loss rates. We find that the older (FOS) *HST* data of the R136 stars (which were obtained without the benefits of sky measurements) suffered from significant nebular emission, which would increase the derived mass-loss rates by factors of ∼ 3, all other factors being equal. We also find several

---

stars in the SMC for which the N III $\lambda\lambda 4634, 42$ and He II$\lambda 4686$ emission "f" characteristics do not appear to follow the same pattern as in Galactic stars. Since He II emission is due to the stellar wind (which will be weaker in SMC for stars of the same luminosity), while N III emission is a complex NLTE effect affected mostly by temperature, it would not be surprising to find that these features do not correlate with each other or with luminosity in SMC stars in the same was as they do in Galactic stars, but theory does not provide a clean answer, and analysis of more stars (both SMC and Galactic) are needed to resolve this issue. The line-blanketed non-LTE atmosphere code FASTWIND was then used to determine the physical parameters of this sample of stars. We find good agreement between the synthetic line profiles for the hydrogen, He I, and He II lines in the majority of the stars we analyzed; the three exceptions show evidence of being incipiently resolved spectroscopic binaries or otherwise spectral composites. One such system is apparently an O3 V+O3 V eclipsing binary, and a follow-up radial velocity study is planned to obtain Keplerian masses. Although we did not use them to constrain the fits, good agreement is also found for the He I $\lambda 3187$ and He II $\lambda 3203$ lines in the near-UV, which we plan to exploit in future studies. Our effective temperatures are compared to those recently obtained by Repolust, Puls & Herrero for a sample of Galactic stars using the same techniques. We find that the Magellanic Cloud sample is 3,000-4,000°K hotter than their Galactic counterparts for the early through mid-O's. These higher temperatures are the consequence of a decreased importance of wind emission, wind blanketing, and metal-line blanketing at lower metallicities.

Subject headings: stars: early-type, stars: atmospheres, stars: fundamental parameters, stars: mass loss

1. Introduction

Translating the observed characteristics of O and early B stars into physical properties has historically proven to be be very challenging. Because of their high effective temperatures, most of their flux is in the far UV, where even spacecraft cannot observe (due to interstellar extinction), as the peak of the flux distribution F_λ will be below the Lyman limit for stars hotter than about 32,000°K. This means that the bolometric corrections are quite significant (-1 to -4 mags), with a steep dependence on the effective temperature. Thus getting the effective temperature right is the key to determining the other physical properties of a hot, massive star.

Since we are always observing the fluxes of these stars far on the tail of the Rayleigh-Jeans distribution, the observed colors of these stars show little sensitivity to effective temperature. For instance, the Kurucz (1992) model atmospheres predict that a dwarf ($\log g = 4.0$) with $T_{\rm eff}$=50,000°K will have $(U - B)_o = -1.151$ and a $(B - V)_o = -0.326$, while a dwarf with $T_{\rm eff}$=40,000°K will have a $(U - B)_o = -1.124$ and $(B - V)_o = -0.311$ (Massey 1998a). The difference in these colors is well within the error of most photometry, and yet the bolometric correction (BC) is -4.5 mag for the former, and -3.8 mag for the latter, using the conversion of Vacca, Garmany, & Shull (1996). This uncertainty in the BC would result in an uncertainty of 0.15 dex in the log of the mass, using the mass-luminosity relation implied by the Schaller et al. (1992) $Z = 0.02$ evolutionary tracks ($L \sim M^2$; see discussion in Massey 1998a). i.e., $50\mathcal{M}_\odot$ vs. $70\mathcal{M}_\odot$. Reddening complicates the interpretation of the photometry further, of course, and although reddening-free indices can be constructed assuming an average reddening law, even an "optimal" reddening-free index using space-craft accessible UV photometry (such as $F170W$) remains too degenerate to be useful (Massey 1998a).

In principle, spectroscopy should allow us to resolve this degeneracy nicely, as the relative strengths of He I and He II (O stars) and Si IV and Si III (early B supergiants) are quite sensitive to the effective temperature (and only secondarily to the $\log g$), as confirmed by non-LTE calculations (Auer & Mihalas 1972; Kudritzki, Simon, & Hamann 1983; Lennon et al. 1991). Indeed, a difference of one spectral subtype (O5 V to O6 V, say) roughly corresponds to a difference in effective temperature of 0.02 dex in $\log T_{\rm eff}$, and a corresponding difference of only 0.13 mag in the bolometric correction, and hence 0.025 dex in the mass of the star ($50\mathcal{M}_\odot$ vs. $53\mathcal{M}_\odot$) one would deduce from the mass-luminosity relationship.

However, the absolute calibration of the relationship between effective temperature and line strengths (or, equivalently, spectral subtypes) requires reliable stellar atmosphere models. Unfortunately, the physics of these stellar atmospheres is quite complicated. The strong lines are all formed under non-LTE conditions, as first shown by Auer & Mihalas (1972), and in addition stellar winds provide a significant source of heating for the photosphere through the backscattering of radiation (Hummer 1982, Abbott & Hummer 1985). Each decade has seen an improvement in our understanding of the physics of these stellar atmospheres, along with the development the numerical techniques to include these effects in a model atmosphere. We identify four stages in the evolution of these models and hence in the effective temperature scale of O-type stars:

1. *The introduction of non-LTE.* The non-LTE models of Auer & Mihalas (1972) and Kudritzki (1975, 1976) were relatively simple by today's standards, in being plane-parallel and including no metals, but in fact required the development of a number of innovative techniques in order to include the effects of non-LTE in line formation.

(See the review by Kudritzki & Hummer 1990). The Auer & Mihalas (1972) models were the first to correctly reproduce the observed line strengths of the helium and hydrogen spectral lines in O-type stars, as was shown by Conti & Alschuler (1971). This led to the first modern effective temperature scale for O stars, that of Conti (1973). This work was extended to the newly defined O3 spectral class (Walborn 1971b) by Kudritzki (1980) and Simon et al. (1983).

2. *The introduction of mass-loss.* Abbott & Hummer (1985) showed that the presence of stellar winds had a significant effect on the He I/He II line ratios and hence on the effective temperatures deduced for O-stars. Although the photospheric lines are formed in a nearly static part of the atmosphere, the scattering of radiation by the stellar winds back into the photosphere results in substantial heating of the surface layers, an effect known as "wind blanketing". This effect is quite significant, as a high (but realistic) mass-loss rate would result in a 42,000°K model matching an O3 V star, while the same model without mass loss would match that of an O5.5 V star. In other words, the greater the mass-loss rate, the cooler the effective temperature is for a given spectral subtype. Conti (1988) revised the effective temperature scale to somewhat lower values, presumably to take this effect into account.

Of special note is the revised effective temperature scale of Vacca et al. (1996), which has generally become the standard against which other work is judged. This scale was based on modeling drawn from the contemporaneous literature, and as such represented the best that the field had to offer at the time. Although it included *some* work that was based on wind-blanketed models, the vast majority of the data was not (e.g., Herrero et al. 1992), and so the derived temperature scale was significantly higher than Conti (1988).

3. *The inclusion of hydrodynamics and metals.* The next decade saw substantial improvements in the modeling, with the introduction of spherical extension and a more sophisticated treatment of the stellar wind as well as non-LTE treatment of the metal lines. Rather than just using the mass-loss rates, the hydrodynamics of the stellar winds in both the sub- and supersonic regions was included. These improvements were pioneered by the stellar atmospheres group in Munich (e.g., the *unified model atmospheres* concept; see Gabler et al. 1989), which used them for the "quantitative spectroscopy of hot stars" (Kudritzki et al. 1989, Kudritzki & Hummer 1990, Kudritzki 1991). (A similar but independent approach was taken by Schaerer & Schmutz 1994, who made the first attempt to include the opacity of metal lines.) Sellmaier et al. (1993) demonstrated that in addition to the effect of wind-blanketing, the stellar winds produced emission that partially filled in the He I lines, which has a strong effect on the effective temperatures as a function of the He I/He II line ratios. Another

seminal work from this period was Puls et al. (1996), who analyzed a large sample of Galactic and Magellanic Cloud O stars using UV and optical data. The UV spectra were used to determine the terminal velocities of the stellar winds using the strong resonance doublets N V $\lambda\lambda 1239, 43$, Si IV $\lambda\lambda 1394, 1403$, and C IV $\lambda\lambda 1548, 51$. The mass-loss rates were then determined primarily by observations at Hα, combined with an assumption (and occasional adjustment) of β, a parameter that characterizes the steepness of the velocity law in the stellar wind (Sec. 3.1). The classical MK optical/blue region (3800Å to 4900Å) still provides the primary diagnostics of the surface gravity (from the hydrogen Balmer-line profiles) and effective temperatures (from the He I and He II lines).

4. *The full inclusion of line blanketing.* A significant improvement in hot star model atmospheres has been the inclusion of full line blanketing. The CMFGEN code, described by Hillier & Miller (1998) and Hillier et al. (2003) is one such example. Originally developed and used for fitting emission-line features in the expanding atmospheres of Wolf-Rayet stars, CMFGEN has been only recently used for the analysis of absorption lines in O-type stars (i.e., Martins, Schaerer & Hillier 2002, Crowther et al. 2002, Hillier et al. 2003, Bouret et al. 2003). Although only a few stars have been fit, these studies suggest that the effective temperature scale of Vacca et al. (1996) is too high[3]. (See also discussion in Martins et al. 2002). Similarly, WM-basic, a code developed by Pauldrach, Hoffmann, & Lennon (2001), includes full line-blanketing, and its use by Bianchi & Garcia (2002) also suggests that a lowering of the effective temperature scale is in order. (WM-basic lacks the Stark broadening and the co-moving frame treatment needed to compute useful synthetic spectra of the quasi-photospheric hydrogen and helium lines, but is very useful to fitting the metal lines found in the UV spectrum.) FASTWIND ("Fast Analysis of STellar atmospheres with WINDS"), first described by Santolaya-Rey, Puls, & Herrero (1997), has now been modified to include an approximate—but highly realistic—treatment of line-blocking, with a similar effect on the effective temperatures (Herrero, Puls, & Najarro 2002, Repolust, Puls, & Herrero 2004).[4]

---

[3] This would be expected in any event given the lack of wind-blanketed model fits in the literature at the time of the Vacca et al. (1996) study.

[4] The use of an *approximate* treatment of line-blanketing and blocking is necessitated by the need for reasonable computational times for a model. We note for comparison that a single run of CMFGEN, with its more rigorous treatment, requires 9 hours on a 1.3-GHz Pentium IV processor, according to Smith, Norris, & Crowther (2002). By contrast, a single run of FASTWIND requires less than 7 minutes on a slower 750-Mhz SparcIII processor on the Lowell workstation we used in this study. In general, something like 10 to 30 models are needed to fit a star. Comparisons of the flux distribution of FASTWIND with those of WM-basic

In this series of papers, we will use new observational data with the latest generation of model atmosphere code to derive a new effective temperature scale for O and early B-type stars, exploring for the first time the effect that metallicity plays on the effective temperature scale (and other derived physical parameters) of these stars. This is crucial for many astrophysical applications, such as deriving the initial mass function from H-R diagrams (Massey 2003), or in modeling expanding shells, super-bubbles, and normal H II regions, where having an accurate census of the ionizing flux and amount of mechanical energy being supplied to the region by stars is crucial (Oey & Kennicutt 1997). The series will eventually encompass hot stars in the SMC, LMC, Milky Way, and the Andromeda Galaxy, which span a factor of 6.8 in metallicities, at least as measured by the oxygen abundances (see Massey 2003 and references therein). Here we begin by studying a sample of hot stars in the Magellanic Clouds. Analysis of a second sample of Magellanic Cloud stars is currently underway, and will be published shortly.

2. Observations and Reductions

We list in Table 1 the identifications and spectral types of the sample of stars we consider here. As previously noted, our modeling requires observations taken in three spectral regions: (1) the 1200-1900Å region where the strong stellar wind resonance lines are found, in order to determine the terminal velocity of the wind; (2) the blue-optical region of the spectrum, where the strong Balmer hydrogen lines determine the effective gravity of the star, and the He I and He II line strengths determine the effective temperature; and (3) the Hα line profile, used to determine the mass-loss rate and the value for β, a measure of the steepness of the stellar wind velocity law (e.g., Puls et al. 1996). In principle, values for all three of these are interdependent, but in practice, a reliable value for the terminal velocity can be determined by simple fitting with very approximate values for the other stellar parameters. Determining of the effective temperature, surface gravity, and mass-loss rate does, however, require simultaneous treatment.

2.1. Photometry

One of the necessary input parameters for the modeling is an accurate knowledge of the star's absolute visual magnitude M_V in order to constrain the stellar radius. Fortunately, with stars in the Magellanic Clouds there is no uncertainty about the relative distances, and

---

(Repolust et al. 2004) and CMFGEN (Herrero et al. 2002) have so far shown very good agreement.

even the absolute distances are now known to reasonable accuracy (van den Bergh 2000). However, our experience is that photoelectric photometry of stars in the Magellanic Clouds is simply not as good as CCD photometry, as the large apertures used in the former often allowed contamination by nearby stars and/or nebular emission. Photometry with CCDs allows local sky subtraction, and the issues of crowding can be dealt with either by the use of small digital apertures or, in extreme cases, point spread function fitting techniques. Accordingly, Massey (2002) obtained UBV photometry of nearly all of the stars in our target list (outside of the R136 cluster) and, coincidentally, of an additional 264,600 stars. We list the catalog number in Table 1; not all of the stars have cross-references in Massey (2002) Tables 4 and 6. The color excesses at $U - B$ and $B - V$ were determined using the intrinsic colors expected for each spectral type (Massey 1998b), and the results averaged, with the assumption that $E(U-B) = 0.72 \times E(B-V)$. For the R136 cluster, the WFPC2 photometry of Hunter et al. (1997) was used by Massey & Hunter (1998) to derive M_V, and we adopt these values here.

2.2. Spectroscopy

In Table 2 we list all of the data directly used in our study. These were obtained from both HST and the CTIO 4-m telescope, and cover the UV, Hα, and optical/blue regions.

2.2.1. Ultraviolet

For all of our program stars, we used HST to obtain spectra in the UV region, where the major stellar wind resonance lines N V$\lambda\lambda1239, 43$, Si IV $\lambda\lambda1394, 1403$, and C IV $\lambda\lambda1548, 51$ are located. Our data came both from archival programs and our own program.

For the ultraviolet observations of the R136 stars we used the archival HST observations made with the Goddard High Resolution Spectrograph (GHRS) by S. Heap (PI) under programs GO-5297 (R136-20=R136a5) and GO-6018 (R136-24=R136a7, R136-36=R136a-608, R136-40=R136a-535, R136-47=R136a-602, and R136-55=R136a-551. The data were obtained in 1994 and 1996, as shown in Table 2, and hence were post-COSTAR. These UV data were the ones used by de Koter, Heap, & Hubeny (1997, 1998), and were obtained with the G140L grating centered at two wavelength settings, 1300Å and 1610Å, and covered the spectral regions 1160-1450Å and 1460-1750Å, respectively. The resolution of the GHRS data is 0.6Å. The observations were made through the 'small science aperture", which was 0.22 by 0.22 arcsec in size.

For the ultraviolet observations of most of the SMC stars, we used the FOS observations made by C. Robert (PI) under program GO-5444. These data were obtained in 1994 and 1995, and were mentioned by Robert (1999) and included in Leitherer et al. (2001). The data were obtained with the G130H grating covering 1140-1606Å, with a resolution of 1.0Å. The data were taken with a 3.7 by 3.7 arcsec aperture.

For AV 296 in the SMC, and the three LMC stars outside of the R136 cluster (LH64-64, LH81-W23, and LH101-W24), we obtained our own UV observations using STIS/FUV under program GO-8633.(Massey, PI). The G140L grating was centered at 1425Å for a wavelength coverage of 1150-1736Å, with a resolution of 0.9Å. The objects were observed through a 0.2 by 0.2 arcsec aperture. In addition, we obtained an observation with the same setup for the SMC star AV 26 (previously observed by Robert 1999 with the FOS) with STIS/FUV under program GO-9412 (Massey, PI). This was intended to serve as a self-consistency check for the terminal velocities obtained with the FOS and STIS.

2.2.2. Optical

For all of the R136 stars we obtained optical data (both blue and Hα) using *HST*. For the rest of the stars, we obtained optical data primarily with the CTIO 4-m telescope. However, in a few cases, where we feared nebular contamination of the Hα profile, or in cases where the stars were very crowded, we supplemented the ground-based data with *HST*.

For the optical (blue and Hα) observations of the R136 stars, we obtained spectra with high signal-to-noise ratios (SNRs) using STIS/CCD. These data were obtained under GO-7739 during 1998 Feb 3-5. These stars had all had previous optical FOS observations by de Koter et al. (1997, 1998) and/or Massey & Hunter (1998), but we knew from our own spectroscopy of R136 stars with the FOS (Massey & Hunter 1998) that the maximum SNR achievable with the FOS was quite limited (typically 60 per spectral resolution element). In addition, we expected that nebular contamination of the Hα profile was likely given the lack of sky subtraction. This indeed proved to be the case, as we show in Sec. 2.3. STIS offered the advantage of a higher SNR plus the ability to subtract nebular emission thanks to the long slit and two-dimensional format of the detector. Nevertheless, the FOS observations are still useful in that they contain spectral lines that are not covered in our STIS observations, particularly He II λ4686, and we make use of the Massey & Hunter (1998) observations for this line. Our blue R136 STIS observations were made with the G430M grating centered at 4451Å, and covering the wavelength range 4310Å to 4590Å, chosen to include Hγ, He Iλ4387, He I λ4471, and He II λ4542. The spectral resolution was 0.4Å. We chose our exposure times to achieve a SNR of 100 per spectral resolution element. The Hα observations were obtained

with the G750M grating, centered at 6581Å, and covering the wavelength range 6300Å to 6850, with a spectral resolution of 0.84Å. Our exposure times were chosen to achieve a SNR of 50 per spectral resolution element. The observations were made with the 0.2×52 arcsec slit. The spatial sampling was 0.05 arcsec pixel^{-1} along the slit. The FOS observations of Massey & Hunter (1998) were made with a 0.26 arcsec diameter aperture, and covered the 3250Å to 4820Å region with 3Å resolution. Those data were obtained under GO-6417 (Massey, PI).

The optical observations for the other stars were mostly obtained during a 5 night run on the CTIO 4-m Blanco telescope with the RC Spectrograph during 3-7 Jan 1999. Grating KPGL-D was used in 2nd order with a $CuSO_4$ blocking filter for observations in the blue (3750-4900Å). The spectral resolution with the 200μm (1.25 arcsec) slit was 1.4Å (3.8 pixels) on the Loral 3Kx1K 15μm CCD behind the blue air Schmidt camera. The slit length was approximately 5 arcminutes, with a spatial sampling of 0.5 arcsec pixel^{-1} (i.e., ten times coarser than with STIS/CCD). For observations at Hα we switched to 1st order and observed from 5400 to 7800Å with a GG420 filter to block 2nd order blue. The spectral resolution for the Hα observations is 2.8Å. In general, conditions were excellent during the run. The stars were well exposed, and by considerable efforts at flat-fielding, we were able to preserve the high SNR of the data, typically 400 to 500 per spectral resolution element. This was a particular challenge in the blue, where exposures of many hours of the dome flat barely achieved a SNR of 100 at 4000Å. Instead, we combined 27 30-sec projector flats to achieve a very high SNR flat suitable for removing the pixel-to-pixel variations, but whose overall illumination function did not match the sky. We corrected the projector flats by using the average of 9 1200-second dome-flat ("Punto Blanco") exposures. Each set of flats was combined with deviant pixel rejection. At Hα it was practical to simply use a series of dome flats to generate an adequate flat-field exposure.

We also have Hα *HST* STIS/CCD observations for two of the non-R136 stars. LH101:W3-24 is located in a region of strong nebulosity, and we were unable to obtain a successful observation from the ground at Hα, and so we observed it with a narrow (0.2 arcsec) slit with *HST* using the G750M with the same setup as used for the R136 stars. For AV26, the same star for which we obtained both STIS and FOS UV observations as a consistency check for the terminal velocities, we also used an observation at Hα as an additional check against our ground-based observation in a "typical" case. Both were observed as part of program GO-9412 (Massey, PI). In order to fill up the remainder of the orbit for each of these two stars, we also observed them in the near-UV region of the spectrum, where the He I λ3187 and He II λ3202 lines are located (see Morrison 1975). These data were obtained with the G430M grating centered at 3165Å, covering 3020-3300Å, with a resolution of 0.4Å. All of the STIS/CCD observations were done in at least two exposures ("cr-split"); in addition, all

but the near-UV observation of LH101:W3-24 were dithered along the slit at three positions in order to increase the SNR.

Three of the program stars (AV378, AV396, and AV451) had no observations at Hα due to on-going problems with the CTIO 4-m control system during the run. We have included these stars in the analysis despite this, making assumptions outlined in Sec. 3

2.2.3. Reductions

The data reduction proceeded as follows. For the *HST* UV observations, all of which were obtained through small apertures, we accepted the *HST* CALSTIS pipeline versions of the reductions. For the *HST* optical (blue and Hα) long-slit STIS/CCD observations, we re-reduced the data *ab initio*, using the recommended flat, dark, and bias frames. We have found that by using the standard spectral reduction algorithms in IRAF[5] (which include optimal extraction and profile-based pixel rejection) we can generally achieve a SNR that is significantly better than that produced by the pipeline. As others may also benefit from our experience, we show the difference in Fig. 1. The SNR of the standard CALSTIS pipeline is worse than that of the re-reduced IRAF data for several incremental reasons. First, good data are lost in the CALSTIS cosmic-ray rejection when the two halves of a "cosmic-ray split" image are combined. The same operation using IRAF can readily be made less aggressive. (Admittedly one could achieve the same result by re-combining the images using the STSDAS implementation of CALSTIS with similar adjustment of parameters.) Second, some of the SNR is lost because CALSTIS fails to do the spectral extraction (summing over the spatial profile) using an optimal extraction routine. With optimal extraction (Horne 1988; Valdes 1992), each point in the profile is summed using a weight that is inversely proportional to the square of the sigma expected on the basis of the read-noise and signal level. Third, IRAF uses the shape of the profile to reject highly deviant pixels (Valdes 1992). As shown in the figure, this is quite effective at reducing the effects of cosmic rays and hot pixels. For shorter exposures, and higher SNR spectra, we found less of a difference, but invariably the IRAF spectrum was to be preferred. The same IRAF extraction routines were used for reducing our CTIO 4-m data.

---

[5]IRAF is distributed by the National Optical Astronomy Observatories, which are operated by the Association of Universities for Research in Astronomy, Inc., under cooperative agreement with the National Science Foundation.

2.3. A Comparison of Our Hα Spectra with Previous Studies

Earlier, we expressed our concern that observations at Hα could give erroneous results in the absence of sky (nebular) subtraction, particularly in dense H II regions such as the one in which the R136 cluster is situated. Contamination by nebular Hα would invariably lead to spuriously large mass-loss rates. The Hα data used in this study have all come from STIS long-slit observations which allow good sky/nebular subtraction. Earlier studies by de Koter et al. (1997, 1998) of R136 though, were forced to rely upon observations made with the FOS and a single aperture. Somewhat suggestively, these studies found that the mass-loss rates of the R136 stars were considerably higher at a given luminosity than that of other O stars that had been studied by Puls et al. (1996). This difference could be real, or it could be due to the different model atmospheres used to derive the mass loss rates—or it could potentially be due to the observations themselves. How well do the older FOS data compare to ours?

The results are shown in Fig. 2. Our STIS (nebular-subtracted) spectra are shown in green, with the FOS (no sky subtraction) spectra used by de Koter et al. (1998) shown in red. In *every* case there is additional emission present in the latter. The fainter stars (R136-040, R136-047, and R136-055) show the larger effect, as would be expected in the case of nebular contamination. For these stars, the FOS spectra fail to even detect the underlying absorption feature, nicely revealed by our sky-subtracted STIS spectra. The de Koter et al. (1998) code did prove its flexibility in being able to match these (spurious) emission features in their stellar modeling. However, in these cases analysis of the FOS would of necessity lead to erroneously high mass-loss rates.

How much of an error would this extra emission introduce? We can provide an approximate answer by taking the parameters we derive for these stars in Sec. 3 and simply increasing the mass-loss rates until we have emission that approximately mimics that of the FOS data. We find that mass-loss rates of 2-4 times what we derive from the STIS data would be needed to approximate the FOS data. (In point of fact we could not get our Hα profiles to match those of the FOS data.) The mass-loss rates we eventually derive for the R136 stars are in fact not that different than those of de Koter et al. (1998) (and in some cases are actually higher!) but this is due to a combination of factors, primarily the much higher temperatures we find from our greater SNR optical data.

Finally, in Fig. 3 we compare our *HST* STIS Hα spectrum of AV 26 to that obtained with the CTIO 4-m. The agreement is quite good, despite the 3.5 times worse resolution of the ground-based data (see Table 2).

3. Analysis

3.1. Terminal Velocities

The first step in our analysis was fitting the UV lines to determine the stellar wind terminal velocities. Terminal velocities were measured from radiative transfer fits of the P-Cygni profile of the C IV $\lambda1550$ doublet. Of the other important resonance lines present in our UV spectra, the shortwards profile of N V $\lambda1240$ is often contaminated by strong interstellar Ly α absorption, making measurements of the terminal velocities from this line very uncertain in most cases. Si IV $\lambda1400$, on the other hand, was often weak, and thus would not allow us precise constraints on v_∞. We have followed the fitting technique described by Haser (1995) (see also Haser et al. 1995), based on the SEI method (cf. Lamers, Cerruti-Sola, & Perinotto 1987). This method has been used in more recent investigations of the UV spectra of Galactic and extragalactic O and B stars, including the HST/STIS work by Herrero et al. (2001), Urbaneja et al. (2002), and Bresolin et al. (2002), to which we refer the reader for details. We allow for a radially increasing turbulent velocity law in the stellar winds, which is described by the usual β parameterization ($\beta \simeq 0.8$ for O stars):

$$\frac{v(x)}{v_\infty} = \left(1 - \frac{b}{x}\right)^{\beta}$$

where $x = r/R$ is the radial coordinate normalized to the stellar radius R, and b fixes the velocity of the inner boundary of the wind to $V(R)$, a value that is of order of the sound speed (Kudritzki & Puls 2000), i.e.,

$$b = 1 - \left(\frac{V(R)}{v_\infty}\right)^{1/\beta}.$$

The best fit to the shortward line profile, which is mostly sensitive to the adopted terminal wind velocity, provided the results summarized in Table 3. In most cases the uncertainties in v_∞ are of the order of 50 to 100 km s^{-1}. Larger uncertainties (up to $\sim$ 200 km s^{-1}) are estimated for those stars having weak C IV lines (noted by the colons appended to their v_∞ value in Table 3), and for which we have also relied on the Si IV lines for estimating v_∞. Typically the maximum turbulent velocity is 9% of v_∞, with values ranging from 3% to 14%.

In Table 3 we also compare our terminal velocities to those of Prinja & Crowther (1998) and de Koter et al. (1998) for the R136 stars in common. In considering this comparison, it is worth noting that the terminal velocities were measured *from the identical data*. In other words, the differences between these measurements are purely due to technique. To the best of our knowledge, this is the first time such a comparison has been carefully performed with the same data. We see that the agreement is fairly good, a few hundred km s^{-1},

consistent with our estimate of our own uncertainty, but far greater than might be naively inferred by the precision with which these measurements are occasionally published. Perhaps fortuitously, our second measurement of the terminal velocity of AV 26 (which was observed both with the FOS and STIS/FUV) agreed to the best of our measuring accuracy. This gives us confidence that the different instrumentation does not introduce much of a bias. We show the CIV lines from the two observations in Fig. 4, along with our modeling of the terminal velocity, as an example.

3.2. Model Fits

The stellar atmosphere code generates synthetic line profiles given the inputs of effective temperature T_{eff}, surface gravity g, the stellar radius R, the mass-loss rate $\dot{M}$, the stellar wind terminal velocity v_∞, the He/H number ratio, and the metallicity $Z/Z_\odot$. For a given model, the parameters $q(\infty)$, q_0, and γ of the non-LTE Hopf function (Santolaya-Rey et al. 1997, Mihalas 1978) must be adjusted until flux conservation ($< 2\%$) is achieved; in practice, this requires several runs. Good starting points for the Hopf parameters were found by interpolating of successful values from previous runs of similar input values.

In fitting a star, we adopted the terminal velocities determined in the previous section, and assumed a metallicity $Z/Z_\odot$ of 0.2 for the SMC stars and 0.5 for the LMC stars[6] A He/H number ratio of 0.10 was adopted, and adjusted if needed. For several stars the helium lines produced by the models were too weak compared to the theoretical hydrogen lines, and we had to increase the He/H ratio, as described below. If the He/H ratio was increased, the relative mass fractions of the other elements were retained. Although this is not quite right (as some elements, such as nitrogen, would likely also increase in abundance, while carbon and oxygen would decrease) it does preserve the overall fraction of metals, particularly the unprocessed Fe group elements, which are most important in the blanketing. An examination of the evolution of the metallicity in the cores of massive stars suggests that this is a good approximation: although the relative proportion of elements changes during core H-burning, the overall fraction of the mass of the star that is in metals changes very little until He-

---

[6]The values for the metallicities are certainly arguable: as Westerlund (1997) notes, the relative abundances of the interstellar medium in the SMC, LMC, *and* the nearby regions of the Milky Way are non-solar. Based primarily on the work of Russell & Dopita (1990), Westerlund (1997) argues that the "average" metal abundance is 0.6 dex and 0.2 dex lower in the ISM of the SMC and LMC than in the solar neighborhood; see also Garnett (1999). The gas in the solar neighborhood is perhaps 0.1 dex lower than that of the Sun (Shaver et al. 1973, Cameron 1982; Table 8 of Russell & Dopita 1990), although recent revisions in the solar abundances may suggest otherwise (Asplund 2003).

burning products are produced[7]. A starting value for the mass-loss rate was estimated by adopting the bolometric correction based on the spectral type using the Vacca et al. (1996) calibration and adding this to the absolute visual magnitude (Table 1) in order to get a crude approximation of the bolometric luminosity L; a mass-loss rate based upon Puls et al. (1996) and scaled appropriately by the metallicity was then used for a first approximation. Following Repolust et al. (2004), we adopted a micro-turbulence velocity of 10 km s^{-1} for the models with effective temperatures of 36,000°K and below, and 0 km s−1 for hotter stars. A grid of 3-9 models using "reasonable" values for the effective temperature and surface gravity (based upon the spectral type and the Vacca et al. 1996 scale) was then run. The initial starting value for the stellar radius was based upon the effective temperature and the approximate bolometric luminosity (using the relationship between the bolometric correction and $T_{\rm eff}$ of Vacca et al. 1996). For each grid point the true radius was then computed using the model flux and effective temperature. If the input and derived radius differed by more than 1%, the input value was adjusted and the grid point recomputed.

After the first series of models is run, a comparison is made by eye between the synthetic spectra from the models and the observed spectrum. For this, both a radial velocity and rotational speed $v \sin i$ must be adopted; these were determined prior to the modeling by examining weak lines in the optical spectrum. In the modeling occasionally this initial measurement had to be slightly refined (by 10%) for a given star. In most cases we found $v \sin i$=110 or 120 km s^{-1}, comparable to the instrumental resolution of the ground-based data, so these values should not be over-interpreted. In general, the wings of the Balmer hydrogen lines Hγ and Hδ are the primary diagnostics of whether the surface gravity is about right, while the relative strengths of the He I and He II lines provide the greatest sensitivity to effective temperature. The Hα profile provides the key diagnostic of the mass-loss rate.

For most of the stars, we achieved excellent agreement between the model synthetic spectra and the observed spectra. However, for three of the stars, no adequate fits could be achieved. We believe this is only to be expected: the frequency of close binary O-type stars in the Milky Way is about 35% (Garmany, Conti, & Massey 1980); in most of these systems, the mass ratio is near unity with the companion another O-type star. If the binary frequency is similar in the LMC and SMC (a subject for which there is little data to argue one way or the other), then we would naively expect about one-third of our sample to consist of stars with composite spectra. One or two additional stars are likely unrecognized composites.

---

[7]Compute the value $Z = 1 - (Y_c + X_c)$ as a function of time in the models of Schaller et al. 1993, for example. One will find for the 120$\mathcal{M}_\odot$ (their Table 1) that metallicity *in the core* changes insignificantly from 0.0082 to 0.0077 during core H-burning. The same numbers are found for a star of 20$\mathcal{M}_\odot$, as found in their Table 6.

Subsequent to our beginning this study, one of the stars (R136-024) for which no good fit could be found was shown to have light variations typical of eclipses (Massey, Penny, & Vukovich 2002), further supporting this interpretation.

Repolust et al. (2004) discuss a long-standing problem with stellar atmosphere codes (see Voels, Bohannan, & Abbott 1989) namely that He I λ4471 (which is one of the principal spectral classification lines) synthetic spectrum is generally *weaker* than that observed in the cooler O-type giants and supergiants among their Galactic sample. This problem is not understood to date, although we are continuing to investigate various causes. Here we can say that we find the same problem as reported by Repolust et al. (2004) for Galactic stars in our lower-metallicity Magellanic Cloud sample. Since the problem seems to only affect the lower-gravity stars cooler than O6, this is in practice not an issue, as for these stars we can rely upon other He I lines which are apparently not affected by this problem, most notably He I λ4387.

Repolust et al. (2004) consider the possibility that the He I λ4471 problem might be resolved by including a more consistent calculation of the temperature structure, including that of the outer part of the stellar wind. We originally used the identical version of FASTWIND as used by Repolust et al. (2004) for making the model fits. Near the end of our study, work on an improved version was completed. This version now includes a self-consistent temperature stratification, in which the equation of thermal balance of electrons is used to derive the temperature structure, except in the innermost region of the photosphere, where a flux correction method is used (see Kubat, Puls, & Pauldrach 1999). In addition, the new version includes a more extensive line list, leading to better fluxes in the UV. We re-ran this improved version on all of our models, and carefully compared the results. Only the fits for the stars with very high mass-loss rates (R136-020 and R136-036) were significantly affected, as we expected. In those cases the new derived temperatures and mass-loss rates were somewhat lower than those produced with the earlier version. No improvement was seen in the agreement for the He I λ4471 line for the problem stars. The numbers and fits given here are all from this newer version; comparison with the Galactic sample analyzed by Repolust et al. (2004) should be valid, as the mass-loss rates are comfortably low, except for HD 93129A, which is a spectroscopic binary and excluded from consideration below.

Given that there is a certain amount of subjectivity in determining the "best fit", what are reasonable uncertainties on the fitted parameters? In general, we found that we could determine effective temperatures with an uncertainty of 1,000°K, and $\log g$ to 0.1 dex. In the cases where we had to increase the He/H ratio from 0.10 in order to get a good fit, we generally were confident of our value to $\pm$0.05, except for LH64-16, for which we find a very high He/H ratio, with an uncertainty that is about 0.1. The uncertainty in $\dot{M}$ is

generally less than 20%, although we caution that our models lack stellar wind clumping, and we expect that this will affect the derived mass-loss rates for stars with Hα in emission, but with minimal impact on the majority of our stars, for which Hα is in absorption (see Repolust et al. 2004). For stars with the lowest mass-loss rates ($< 3 \times 10^{-7} M_\odot$ yr^{-1}) we include both the value used in the fit and the upper limit (under "Comments") in Table 4.

3.3.   Spectral Classification Issue at Low Metallicity.

In general, we followed the precepts of the Walborn & Fitzpatrick (1990) atlas in (re)classifying the stars. The basis for the spectral subtype is primarily the ratio of the He I to He II ratios, particularly that of He I λ4471 and He II λ4542 (cf. Conti & Alschuler 1971). For stars that would have been classically classified as "O3", we used the criteria given by Walborn et al. (2002a) to classify these stars as either O2 or O3. In addition to assigning a spectral subtype on the basis of the overall *appearance* of the spectrum (compared to the Walborn & Fitzpatrick 1990 atlas), we also *measured* the equivalent widths of the He I λ4471 and He II λ4542 lines, and compared the ratio to that used to define the spectral subtypes by Conti & Alschuler 1971). Below we quote the quantity $\log W' = \log W(4471) - \log W(4542)$, where W is the equivalent width. In practice, there were no differences between the two methods.

Assigning the luminosity class to these stars is slightly trickier. The amount of emission in N III λλ4634, 42 and He II λ4686 results in an "f" designation, with the spectroscopic description "((f))" referring to weak N III emission and strong He II λ4686 absorption. The description "(f)" refers to N III emission with partially filled in He II absorption, while "f" refers to both features being in emission. In the Milky Way the "f"s are invariably supergiants (i.e., "If" stars), while the "(f)" are giants (i.e., "III(f)"), and the "((f))" are invariably dwarfs (i.e., "V((f))"). But at low metallicity, such as found in the SMC, this shouldn't necessarily follow. The amount of emission in He II λ4686 is a complex function of what is happening in the stellar wind (Klein & Castor 1978, Gabler et al. 1989). The physics involved in the formation of this line is simply not as well understand, say, as that Hα. The formation of Hα will be largely unaffected by blocking in the EUV, while HeII λ4686 may be strongly affected, due to the importance of the HeII λ303 resonance line in its formation. We could argue equally well that one might expect *more* emission, or *less* emission, for stars of the same luminosity and effective temperatures. Similarly, the emission in N III λλ4634, 42 is a complex NLTE effect, and its size to large extent dependent upon the effective temperature (Mihalas & Hummer 1973; Taresch et al. 1997). Without any stellar wind, He II λ4686 would be in absorption in stars of all luminosity classes, while N III would

still show emission. Thus, it is not unreasonable to expect that the "f" properties of a star may not follow our Galactic prejudices as we look at O stars at lower metallicities. We will therefore call attention to the M_V when discussing the stellar classifications, as abhorrent as this practice may seem to classification purists.

Of course, one can always argue that any particular star with a discrepantly high visual luminosity may be a spectroscopic binary. At the distances of the Magellanic Clouds such blends might not even be revealed by radial velocity motion, given that 1" projects to 0.24 pc (LMC) or 0.29 pc (SMC). However, below we find several examples (AV 26, AV 75, and possibly AV 469) where the "f" characteristics are not consistent with the star's M_V in the SMC, but none in the LMC. To explain these away as binaries would require our SMC sample to be biased towards unresolve multiple systems in a way that the LMC sample is not. While not impossible, the alternative explanation that we are seeing a metallicity effect on the "f" characteristics generally used to define the luminosity class, would appear to us as more attractive.

3.4. Comments on Individual Stars

In this section we discuss the derivation of the spectral types, and present the results of our model fits. The physical parameters are given in Table 4. We include in that table the so-called "spectroscopic mass", $M = g/g_\odot \times R^2$. In the figures showing the spectra, occasional bad columns have been removed by linear interpolation.

3.4.1. SMC

AV 14. AV 14 was first classified as "O5 + neb" by Ardeberg & Maurice (1977), and reclassified as "O3-4 V + neb" by Garmany, Conti, & Massey (1987). Its early spectral type resulted in its inclusion in our program. The "+ neb" designation often came about due to photographic spectral classification of early-type stars in the Magellanic Clouds, as local sky subtraction was not possible as it is with CCD spectrometers. Here we reclassify the star as O5 V. The visual appearance of the spectrum (Fig. 5a) is consistent with the measured ratio of the equivalent widths, $\log W' = -0.57$. The absolute visual magnitude of this star, $M_V = -5.8$, would suggest it is intermediate between luminosity class "V" and 'III", according to Conti (1988); however, by comparison to any Galactic standards, the luminosity class is clearly "V", as He II $\lambda4686$ is strongly in absorption. The spectrum is a very good match to that of Walborn & Fitzpatrick's (1990) spectrum of HD 46150, although

there is no hint of N III $\lambda\lambda 4634, 42$.

We obtained good fits after just a few models (Fig. 5b). In this case, the He I $\lambda 4387$ line strength would suggest a slightly lower temperature (42000°K) than the one we adopt here. However, this lower temperature produces He II lines which are weaker than observed. The He I $\lambda 4471$ line shows good agreement with the fits based upon He II. The mass-loss rate is low, and therefore not very well determined, with adequate fits obtained with values $\dot{M} \leq 3 \times 10^{-7} M_\odot$ yr^{-1}.

AV 26. AV 26 was classified as an O7 III by Garmany et al. (1987). Here we classify it as just slightly earlier, O6, based upon the visual impression of the spectrum (Fig. 6a) We also measure $\log W' = -0.22$, consistent with the O6 spectral type. As for the luminosity class, the star's absolute visual luminosity ($M_V = -7.0$) requires it to be a bright supergiant. A Galactic O6 star of this luminosity, though, would have very strong N III $\lambda\lambda 4634, 42$ and He II $\lambda 4686$ emission. Instead, we see weak N III emission and slightly weakened He II $\lambda 4686$ *absorption.* Nor would we expect to see N IV $\lambda 4058$ emission in an O6 star of any luminosity type. Are these peculiarities due to the low metallicity characteristic of the SMC, or are we seeing a composite spectrum? The presence of N IV emission in Galactic O-type stars is invariably either coupled to strong He II $\lambda 4686$ emission (in an O3-4 I), which we don't see, or to N V absorption (in an O3 III), which we also don't see. (N IV $\lambda 4058$ in dwarfs is weaker than what we detect in our spectrum, -70mÅ.) Given this, we tentatively rule out the composite explanation[8]. We believe the spectral features we see in AV 26 are just normal for an O6 I star in the low metallicity environment of the SMC. We classify this spectrum as O6 I(f). The following star (AV 75) provides an additional example. Unless the star *is* a composite spectral type, then the behavior of the N III and N IV selective emission lines underscores the dangers of interpreting these line ratios as an effective temperature indicator, as was recently done by Walborn et al. (2002a, 2004).

We judge the fits of the model to the observed spectrum good. These are shown in Fig. 6(b). The surface gravity is $\log g = 3.5$, consistent with the supergiant designation. AV 26 is one of the two stars for which we also have near-UV data for the He I $\lambda 3189$ and He II $\lambda 3203$ lines. We will introduce these powerful diagnostic lines in Section 4.

AV 75. AV 75 was classified as an O5 III(f) star by Garmany et al. (1987), and as O5 III(f+) by Walborn et al. (2000), who make reference to its "entirely normal hot O giant spectrum" in both the optical and UV. Our spectrum (Fig. 7a) agrees well with the "O5"

---

[8]We are grateful to Nolan Walborn for correspondence on this subject, although our final conclusion differed from his, primarily because at our high SNR (350 per 1.2Å resolution element) we can place a very stringent upper limit on the presence of any N V absorption.

designation, and we measure $\log W' = -0.38$. However, at $M_V = -6.9$ the star must be considered a supergiant but with He II $\lambda 4686$ in absorption rather than emission due to the smaller stellar wind that comes from lower metallicity. The "+" designation signifies that Si IV $\lambda 4116$ is in emission, a result which we also confirm. Like Walborn et al. (2000), we note that the Si IV $\lambda 4089$ line is very weakly present in absorption, a result which we find somewhat curious despite Walborn et al. (2000)'s explanation. We classify the star as O5.5 I(f+). Good agreement is found is found with the model fits (Fig. 7b).

AV 207. Our spectrum (Fig. 8a) of AV 207 shows He I $\lambda 4471$ is just slightly stronger than He II $\lambda 4542$ in this star, making it of spectral type O7.5. We measure $\log W' = +0.03$. N III is very weakly in emission, with He II $\lambda 4686$ absorption strong, and so we designate the star as "((f))". The absolute luminosity ($M_V = -5$) is consistent with the star being of luminosity class "V" (i.e., Conti 1988). Previously the star was classified as O7 V by Crampton & Greasley (1982), in good agreement with our determination of O7.5 V((f)). A good fit (Fig. 8b) was found for all of the lines. The mass-loss rate for this star is low, with values $\leq 3 \times 10^{-7} M_\odot \text{ yr}^{-1}$ yielding good fits.

AV 296. At first glance (Fig. 9a), AV 296 appears to simply be a broader-lined version of AV 207. We classify it it similarly as O7.5 V((f)) visually, and measure $\log W' = +0.05$, consistent with that spectral subtype. The absolute visual magnitude is very similar ($M_V = -5.1$) to that of AV 207. The star was previously classified as "O5 V:" by Garmany et al. (1987), with the ":" denoting an uncertain type due to nebular contamination.

We obtained a barely adequate fit (Fig. 9b) to the spectrum. The required surface gravity $\log g$ is low, more characteristic of a supergiant than a giant or dwarf. Possibly this is an effect of the rapid rotation lowering the effective surface gravity, but we suspect that this star may be a spectroscopic binary with not-quite-resolved double lines at the time of the exposure. This view is further supported by the measured radial velocity of the star, $\sim 250 \text{ km s}^{-1}$, which is quite high given the 158 km s^{-1} systemic velocity of the SMC (see Fig. 1 of Massey & Olsen 2003). A radial velocity program is probably warranted, but for now we include the derived values in Table 4 but note this uncertainty.

AV 372. We originally classified this star as an O9.5 I (Fig. 10). Walborn et al. (2002b) arrived at a similar type ("O9 Iabw"). The supergiant status is suggested not only since $M_V = -6.8$ but also due to the strength of Si IV absorption. However, we were unable to find any simultaneous good agreement of the strengths of both He I and He II. In addition, the Hα profile appears to be P Cygni, and no amount of tweaking of the mass-loss rates and β (from 0.5 to 2.5) produced an acceptable fit at the temperatures indicated by the He I to He II ratios. The Balmer line profiles were suggested of very low surface gravity ($\log g = 3.2$), and at first we thought that we had encountered a problem with the models. However, further

inspection of the optical spectrum revealed that the He I lines were significantly *broader* than the He II lines. We measure a $v \sin i$ of 110 km s^{-1} for He II but require a $v \sin i$ of 200 km s^{-1} for He I. The centers of He I lines are also shifted by -20 km s^{-1} with respect to those of He II. The star is likely a spectroscopic binary, with two stars contributing to He I and one star dominating the He II spectrum.

AV 377. The spectrum (Fig. 11a) appears to be that of an O5 V((f)), with slightly anomalously strong N III $\lambda\lambda4634, 42$ emission. Even visually, however, we see that the He II lines are rather strong compared to hydrogen, in comparison to the Walborn & Fitzpatrick (1990) atlas. We measure a value of $\log W' = -0.55$, consistent with the O5 spectral subtype. The absolute magnitude, $M_V = -4.9$, is consistent with the luminosity class "V" designation. Previously, the star was classified as O6 V by Garmany et al. (1987).

Fitting this star required increasing the He/H number ratio from the canonical value 0.10 to a considerably higher value: 0.35. When we did this we obtained simultaneously good fits to the He I, He II, and Balmer lines (Fig. 11b). The only exception was He II $\lambda4542$, for which the model line was weaker than the observed line. However, the fits at He II $\lambda4200$ and He II $\lambda4686$ were good. Increasing the temperature slightly does not improve the fit to He II $\lambda4542$ and makes the model He I spectra too weak. Similarly, either a slighter lower value (0.3) or higher value (0.4) for He/H produced He lines that were too weak or too strong, respectively.

It has become increasingly recognized that rotation can play an important role in enriching the surface material even during the main-sequence stage (Maeder & Meynet 2000, Walborn et al. 2004). The enriched He abundance is likely consistent with the stronger-than-expected presence of N III $\lambda\lambda4634, 42$ emission. The low mass-loss rate we find for this star ($\dot{M} \sim 10^{-7} M_\odot$ yr^{-1}, with only an upper limit $\dot{M} \leq 3 \times 10^{-7} M_\odot$ yr^{-1} firmly established) is surprising given its spectral type, but is consistent with the UV spectrum, for which the stellar wind lines were quite weak.

AV 378. We classify this star as spectral type O9.5 III (Fig. 12a) with guidance from the referee Nolan Walborn, who argues that He II absorption is consistent with a giant classification. We initially preferred a supergiant designation. The spectral subtype is consistent with $\log W' = +0.47$. We find $M_V = -5.5$, which is halfway between what we expect for a giant and supergiant. The star has been previously classified as O8 V by Garmany et al. (1987).

The surface gravity of this star is relatively low ($\log g = 3.25$), which is much more consistent for a supergiant than that of a giant. We quickly found that we needed to slightly increase the He/H ratio to obtain an adequate fit for both the He I and He II lines (Fig. 12b).

For this star, the He I $\lambda4471$ and He II $\lambda4387$ lines were inconsistent, in the same sense as described by Repolust et al. (2004), i.e., the model spectrum of He I $\lambda4471$ is too weak at lower temperatures in giants and supergiants. Accordingly we have relied upon the He I $\lambda4387$ and to a lesser extent on the He I $\lambda4922$ line (not illustrated) in determining the fit.

This star did not have any measurable stellar wind lines, and so we simply adopted a value of $v_\infty = 2000$ km s^{-1} in computing its models. We lack data at Hα, but began with the initial assumption that the mass-loss rate was quite low ($10^{-7}M_\odot$ yr^{-1}). Examination of the He II $\lambda4686$ profile then suggested that $\dot{M}$ was even lower, and we adopted a value based upon the fitting of this line. The temperature, surface gravity, and He/H ratio are all very well determined in this regime.

AV 396. We classify the spectrum of AV396 as B0 III (Fig. 13a). The spectral type is clearly later than that of AV378 (O9.5 III). Classically, the dividing line between O9.5 and B0 was the presence or lack of He II in the spectrum (Jaschek & Jaschek 1990), but higher signal-to-noise spectra now results in stars of B0 type having detectable He II $\lambda4200$ and He II $\lambda4542$ as well as the strong (luminosity-dependent) He II $\lambda4686$ line. If v Ori (HD 36512) is considered a B0 V, as all authors have done since Johnson & Morgan (1953), then we would conclude that the spectral type of AV396 is also B0. A later type (such as B0.2, as introduced for τ Sco by Walborn 1971a), can be ruled out based upon the fact that Si IV $\lambda4089$ is strong but Si III $\lambda4552$ is all but non-existent, while these lines are of comparable strengths in τ Sco[9]. Since we can determine the physical parameters of this star based upon the He I to He II ratio, we consider the "B0" spectral type an honorary member of the O-type class. A comparison of the properties derived in this way will be made to what we obtain using the Si IV to Si III lines in a subsequent paper. The absolute magnitude of the star, $M_V = -5.2$, is consistent with it being a giant, although (as expected) the Si IV lines are weaker with respect to He I what we would find in a Galactic giant. (Compare Fig. 13a with the spectrum of HD 48434 shown in Fig. 17 of Walborn & Fitzpatrick 1990). Previously the star was classified as O9 V by Garmany et al. (1987), doubtless due to the (weak) presence of He II.

We did not detect any measurable stellar wind lines in the UV, and we lack an Hα spectrum of the star. We again assume a minimal mass-loss rate and a terminal velocity $v_\infty = 2000$ km s^{-1} in making the fit. We judge the fits shown in Fig. 13b excellent, with the

---

[9]Here we forced to eschew the intermediate class O9.7 introduced by Walborn (1971a) and used by Walborn & Fitzpatrick (1990). First, this intermediate class is defined only for supergiants, and secondly, it is based upon the ratio of the He II $\lambda4542$ to Si III $\lambda4552$ lines. The strength of the latter is not only gravity-dependent, but the strength relative to He II will also depend heavily on the metal-content of the star.

values of T_{eff}, $\log g$, and He/H well determined. (We did have to increase He/H to 0.15 to obtain a good fit.) The model He I $\lambda 4471$ line is again weaker than expected compared to the other He I lines, primarily He I $\lambda 4387$.

AV451. The spectrum of this star (Fig. 14) is clearly earlier than that of AV396 (Fig. 13), and very similar to that of Fig. 12, except that the luminosity indicator Si IV to He I is much weaker than in AV378. We classify this spectrum as O9.5 III, consistent with $M_V = -5.2$ Previously this star was called an O9 V by Garmany et al. (1987).

Again, we were not able to discern any stellar wind lines in our UV spectrum of the star, and we lack an observation of the Hα profile. We assume a minimal mass-loss rate $(10^{-7} M_\odot \ \mathrm{yr}^{-1})$ and terminal velocity $v_\infty = 2000$ km s^{-1} in making the fit.

Our first attempt at modeling the spectrum of this star, however, revealed that it is a likely double-lined spectroscopic binary: the He I lines are much broader ($v \sin i = 200$ km s^{-1}) than the He II lines ($v \sin i = 120$ km s^{-1}), suggesting that this system consists of a mid-O and late-O pair of stars. No satisfactory combination of surface gravity and rotational velocities could match the Balmer lines. We add this to our list of stars that deserve radial velocity monitoring.

AV469. The spectrum of this star is readily classified as O8.5 I(f), with the only spectral peculiarity being that He II $\lambda 4686$ is in absorption, while in a Galactic O8 I star of comparable M_V we would expect it to be mostly filled in by emission (e.g., HD 17603; see Conti & Alschuler 1971). Otherwise, the spectrum is very similar to that shown by Walborn & Fitzpatrick (1990) for HD 151804 (O8 Iaf), including the strong N III absorption features at 4097Å and 4511-15Å(Fig. 15a). We measure a value of $\log W' = +0.24$, which suggests the intermediate (O8.5 rather than O8) type. The absolute visual magnitude of the star, $M_V = -6.2$, is consistent with its supergiant designation. Previously, this star was classified as O8 II by Garmany et al. (1987), and as O8.5 II((f)) by Walborn et al. (2002b).

Despite running 28 models for this star, we were left unsatisfied with the final fit (Fig. 15b). In particular, the Hα line has a small emission bump which we were unable to reproduce despite our exploration of parameter space (both β and $\dot{M}$). In addition, the velocity of the synthetic He II $\lambda 4686$ line is clearly shifted to the blue relative to the observed line. Nevertheless, values of T_{eff} and $\log g$ seem well determined. He I $\lambda 4471$ was much weaker in the synthetic spectrum than in the observed spectrum, consistent with our experience that this occurs at low surface gravities and relatively "cool" temperatures.

3.4.2. The non-R136 LMC Stars

LH64-16.[10]. Massey, Waterhouse, & DeGioia-Eastwood (2000) classified LH64-16 as "O3 III:(f*), where the "*" notation denotes that N IVλ4058 emission is stronger than N III $\lambda\lambda$4634, 42 emission, which is generally a characteristic of O3 supergiants (Walborn & Fitzpatrick 1990). We illustrate the spectrum in Fig. 16a. Although "classically" the O3 spectral type is one which lacks He I absorption (Walborn 1971b, Conti 1988), high SNR data can reveal weak ($W =\sim$ 75 to 250 mÅ) He I λ4471 (Kudritzki 1980, Simon et al. 1983). We do detect He I λ4471 very weakly in our spectrum; the measured strength is about 100mÅ.

The absolute visual magnitude of LH64-16 is only −5.2, which would suggest it is a dwarf. However, there is a general problem with this argument when applied to a degenerate spectral class. A 55,000°K O star (were such an object to exist) and a 48,000°K O star would both be classified as "O3" (as they would lack significant He I). If they had the same bolometric luminosity, then the hotter star would be visually fainter. (Since stars evolve at fairly constant $M_{\rm bol}$ this situation could apply simply to the same star at two slightly different ages; the fainter, hotter star would be the younger.) Thus if LH64-16 were a particularly hot O3 star, then it could well be of luminosity class III. From a morphological point of view, there are conflicting data on the luminosity criteria: the strength of N V $\lambda\lambda$4603, 19 absorption, and N IV λ4058 emission would argue this is a supergiant, while the presence of He II λ4686 absorption would argue that it is a giant or a dwarf.

Walborn et al. (2002a) used our spectrum of the star to help define a new spectral class: that of O2. This was based on the relative strength of N IV λ4058 and N III $\lambda\lambda$4634, 42 emission and N V λ4603, 19 absorption. The implications are, of course, that O2 is a "hotter" spectral type than O3, but the interpretation is complicated by the fact that the N lines are luminosity (gravity?) dependent. Walborn & Fitzpatrick (1990) nicely illustrate this in their Fig. 8. There is not a good theoretical underpinning of this new spectral type, as yet. Walborn et al. (2002a) consider LH64-16 to be of an O2 III(f*) star.

The situation has been further complicated by the discovery that LH64-16 is nitrogen-enriched. Walborn et al. (2004) produce yet another new spectral designation, namely ON2 III(f*) to describe the spectrum. Their modeling of our spectrum suggests a some-what enhanced He/H number ratio (0.25) and extremely high temperature (55,000°K), where model fits were obtained by CMFGEN using the near-UV and optical spectrum. (Values of

---

[10]Note that this star has sometimes been referred to as "W16-8", as it is also star 8 in Field 16 of Westerlund (1961). The LH64-16 designation is from Lucke (1972). A hybrid version of the name, "LH64W8", was unwisely used as the designation for the *HST* observations.

surface gravity were adopted, so the issue of luminosity class remains unresolved.) The very high temperature is unprecedented for a model fit with fully-blanketed models.

Our own modeling of this star is shown in Fig. 16b, where we have fit only the optical lines. We found that we needed a high He/H ratio if we were to get the model He II lines as strong as what is observed, and we were forced to increase the He/H ratio to 1.0 to obtain a satisfactory fit. Once we had increased the He/H ratio, though, we needed a very high effective temperature in order to make the He I lines as weak as that observed. Our value for the surface gravity is well constrained (as usual) by the wings of the Balmer line profiles to $\log g = 3.9$, suggesting that it may be a dwarf. The He II λ 4686 profile is very sensitive to the mass-loss rate, and the value we derive from Hα gives a reasonably good fit. Given that Walborn et al. (2004) were also able to model the atmospheric abundances, including the variations of CNO with CMFGEN, their parameters may be better determined than ours, although the source of the disagreement in the He/H ratio (our 1.0 vs. their 0.25) is hard to understand, especially given the fact that they were forced to a similarly high temperature in order to fit the star. They present this star as a possible example of "homogeneous evolution"—that somehow, possibly due to rapid rotation, the star has evolved chemically in such a way that the surface composition is similar to that of the core. The nitrogen enhancement found by Walborn et al. (2004) is a factor of 7 over the presumed starting value. This much nitrogen is consistent with any He/H ratio from 0.25 to 2.0, as it is simply the CNO-burning equilibrium ratio (see Massey 2003 and references therein.)

Our modeling generally supports their results, although not necessarily their interpretation. We find a "spectroscopic mass" ($M \sim g/g_\odot \times R^2$) of $26M_\odot$. A similar value is necessitated by the model of Walborn et al. (2004). Yet, the "evolutionary mass" found by Walborn et al. (2002a) is much higher, $72\mathcal{M}_\odot$, based upon the (non-rotation) evolutionary models of Schaerer et al. (1993). Although for some time there were hints of a mass discrepancy between the spectroscopic and evolutionary masses, improvements in the models (both atmospheric and evolutionary) have largely eliminated this problem (Repolust et al. 2004 and references therein). We will revisit this topic in the second paper in this series. However, here we offer the suggestion that the relatively low mass inferred by the atmosphere modeling (both ours and that of Walborn et al. 2004) is connected to the high chemical abundances found at the surface. Possibly this star is the result of binary evolution, or some other peculiarity. We are indebted to Nolan Walborn for calling this discrepancy to our attention.

LH81:W28-5. The spectrum of LH81:W28-5 (Fig. 17a) is readily classified as O4 V((f+)), with $\log W' = -0.68$. The presence of weak N V 4603,19 absorption is consistent with this classification. The "+" designation denotes the presence of Si IV $\lambda\lambda 4089, 4116$ emission.

Si IV emission is not seen in the example of an O4 V((f)) star shown by Walborn & Fitz-patrick (1990), but our data are of higher SNR, and indeed the Si IV emission features are seen in the Galactic star HDE 303308 described as O4 V((f+)) by Walborn et al. (2002a). The faint absolute visual magnitude ($M_V = -5.0$) is consistent with the strong He II λ4686 absorption feature in determining the "V" luminosity class. Walborn et al. (2002a) cites this star as a representative of the O4V((f+)) class.

Our fit of the parameters of this star was straight-forward, other than the fact the He/H ratio had to be increased slightly in order to produce He II lines as strong as those observed. We judged the agreement between the models and the observations very good, and show the comparison in Fig. 17b.

LH101:W3-24[11]. Our ground-based spectrum of LH101:W3-24 (Fig. 18a) is strongly contaminated with nebular emission lines at the Balmer lines, despite our best efforts to avoid them by narrowing the slit and attempting various regions for sky subtraction. We were fortunate to be able to supplement our ground-based data with exposures both in the near-UV and at Hα with *HST*, allowing us to use a very narrow (0.2 arcsec) slit. (We will discuss the near-UV spectrum below in Sec. 4.) Previously, the spectrum had been classified as O4 V by Testor & Niemela (1998), presumably because He I λ4471 is very weakly present. We measure an equivalent width of 120mÅ for this line, placing it in the same regime as other O3 stars. We thus retain the O3 V((f)) designation of Massey et al. (2000).

Fortunately, the strong nebular lines did not interfere with the fitting: our uncontaminated *HST* Hα spectrum was used to determine the mass-loss rate, while the ground-based Balmer line observations served adequately for the determination of $\log g$, which after all is based upon the fits to the Balmer wings.

We obtained adequate fits, although we did have to slightly increase the He/H ratio from 0.10 to 0.15 to make the He II lines sufficiently strong. There was some disagreement between He II λ4200 and He II λ4542, and we arrived at a compromise. The spectra are somewhat more noisy than most due to the need for a narrow extraction aperture to reduce the effects of the nebular emission. In addition the He II λ4200 line is compromised somewhat due to a bad column which sat on the red wing of the profile. Nevertheless, the overall agreement (Fig. 18b) is good.

---

[11] This star was also cataloged as ST5-27 by Testor & Niemela (1998). It was observed with *HST* under the *nomme de plume* "LH101W24".

3.4.3. The R136 Stars

The spectroscopic study of R136 by Massey & Hunter (1998) identified more O3 stars than had been previously known in total elsewhere. The FOS spectra that were used for that study were of relatively poor SNR, and suffered from intermittent behavior of some of the diodes, limiting the ability to flat-field well. As described in Sect. 2.2, we obtained higher quality data with STIS in a follow-up study designed to allow the modeling we now describe. However, the STIS data covered only a very limited wavelength range (from Hγ through He II λ4542). In what follows we make use of the older FOS data in describing the overall spectrum (and determining the spectral type), but restrict our modeling only to the STIS data. The fits to the FOS's He II λ4686 observations are shown, however, for comparison. In presenting the blue-optical spectra, we have spliced in the better STIS data in the wavelength region 4310Å to 4590Å.

R136-020. This star was classified as O3 If*/WN6-A, with the "slash" designation a tribute to the very strong emission features at N IV λ4058 and He II λ4686, with strengths and widths comparable to those produced in the stellar wind of a Wolf-Rayet star. A comparison of Fig. 19a with that of the O3 If* star HD 93129A shown in Walborn & Fitzpatrick (1990) shows that this is simply a more extreme example, and classically one could drop the "slash" part of the designation and simply call the star an O3 If*. The star was left off the list of O3 stars by Walborn et al. (2002a) due to its "slash" description. However, by their classification criteria it would be called an O2 If*, given the strength of N IV λ4058 emission and the lack of any He I absorption or N III emission. The absolute magnitude $M_V = -6$ is consistent with the star's supergiant designation.

Despite the high mass-loss rate implied by both Hα and He II λ4686, the fitting of this star was straight-forward, and good matches were achieved. A slightly elevated He/H ratio was needed in order to make the He II λ4542 line as strong as observed. He Iλ 4471 is not detected even in our high SNR spectrum, and thus the effective temperature (and hence bolometric luminosity) given in Table 4 must be considered a lower limit.

R136-024. This star was classified as O3 III(f*) by Massey & Hunter (1998); its spectrum is shown in Fig. 20. We were unable to obtain a good fit, and the broadness of the spectral lines suggests it is an incipiently resolved double-lined binary. Indeed, after we began this project, Massey et al. (2002) found light variations that were typical of eclipses. Given the weakness of He I in the spectrum, this system likely consists of two O3 V's, and thus is a good candidate for radial velocity studies with *HST*. Such a project is being proposed.

R136-036. This star was classified as O3 If* by Massey & Hunter (1998); its spectrum is shown in Fig. 21a. The spectrum shows the same luminosity features of the O3 If* star

R136-020, i.e., strong NIV $\lambda4058$ and He II $\lambda4686$ emission, and N V $\lambda4603, 19$ absorption. Walborn et al. (2002a) refer to this as an "O2-O3 If*" star under the designation "MH36". The ambiguity in the spectral type was due to the noisy region around He I $\lambda4471$ in the FOS spectrum; with our higher SNR STIS spectrum, they would undoubtedly have considered this an O2 If* star given the lack of He I and the fact that the N IV emission is so much stronger than any possible N III $\lambda\lambda4634, 42$ emission. We adopt this designation here, despite our ambivalence about the use of selective emission features to extend the spectral classification.

Our fits of Hγ and He II $\lambda4542$ are quite good; the effective temperature given in Table 4 is the lowest for which we obtain a sufficiently weak He I $\lambda4471$ line, and thus must again be considered a lower limit. Although we investigated a broad area of parameter space (β and $\dot{M}$) we did not obtain good fits to the stellar-wind sensitive lines Hα and He II $\lambda4686$. Possibly this is a consequence of the lack of wind clumping in our models, as Hα is strongly in emission.

R136-040. This star was classified as O3 V by Massey & Hunter (1998); its spectrum is shown in Fig. 22a. Since neither NIV $\lambda4058$ nor N III $\lambda\lambda4634, 42$ emission is visible, we would be hard-pressed to classify the star using the scheme of Walborn et al. (2002a). There is no He I λ 4471 detected in this spectrum.

In order to produce He II $\lambda4542$ as strong as what is observed, we must increase the He/H ratio to 0.2. That then requires a very high T_{eff} to match the stringent limit on the He I$\lambda4471$ line. Again this effective temperature should be treated as a lower limit, since no He Iλ 4471 is actually detected, despite the excellent SNR (150 per 2-pixel resolution element) and resolution of our data.

R136-047. This star was classified as O3 III(f*) by Massey & Hunter (1998); its spectrum is shown in Fig. 23a. Despite the higher SNR data at He I λ 4471, no trace of this line could be found. The giant luminosity class is due to the presence of N IV $\lambda4058$ emission. By the criteria of Walborn et al. (2002a), this would have to be called an O2 III(f*) star. We obtained good matches of the model spectrum to the observed spectrum for this star (Fig. 23b), but the fit required a very high effective temperature (T_{eff}=51,000°K) in order to make the model He I $\lambda4471$ line sufficiently weak. Even so, we must consider this a lower limit, since *no* He I $\lambda4471$ is detected in our spectrum. Although we explored much of parameter space (30 models), we never found a combination of β and $\dot{M}$ that produced as good a fit to the Hα profile as we would have liked.

R136-055. This star was classified as O3 V by Massey & Hunter (1998); its spectrum is shown in Fig. 24a. Weak He I $\lambda4471$ is present, allowing an accurate effective temperature to be determined. We were able to fit the spectrum of this star very straight-forwardly

(Fig. 24b), deriving a high effective temperature and a surface gravity consistent with its being a dwarf.

4. Introducing the He I $\lambda3187$ and He II $\lambda3203$ Diagnostic Lines

Morrison (1975) described coudé observations of the He I $\lambda3187$ and He II $\lambda3203$ lines in O and early B-type stars made from the high altitude of Mauna Kea. She motivated this discussion by noting that the He II $\lambda3203$ absorption line ($n = 3$ to 5) provided a unique opportunity to test stellar atmosphere models, as it was the only accessible He II line that did not involve $n = 4$ (i.e., all of the Pickering lines arise from $n = 4$; e.g., He II $\lambda4200$, $n = 4$ to 11; $\lambda4542$, $n = 4$ to 9). Given the presence of emission at He II $\lambda4686$ ($n = 4$ to 3) in many O-type supergiants, Morrison (1975) argued that the $n = 4$ level is overpopulated, at least in some parts of the stellar atmosphere for some stars, although today we would instead say that the emission is simply a pure wind effect, due to the large contributing volume, and has nothing to do with overpopulation. Morrison (1975) found that the He II $\lambda3203$ line was much weaker than predicted by the plane-parallel non-LTE models of Auer & Mihalas (1972) for the stars in which He II $\lambda4686$ is in emission, although reasonable agreement was found in the other cases. The He I $\lambda3187$ line falls in the same spectral region but there were no theoretical predictions for the strength of this line at the time.

We are unaware of any follow-up of this interesting work, doubtless due to the difficulty of observing this wavelength region from the ground. Despite the numerous observations of OB stars with *IUE* (in operation from 1978 to 1996), no new studies of this line were made, probably due to the proximity of the He II $\lambda3203$ line to the long-wavelength cut-off. However, this wavelength region is easily observed with *HST*. We have long been intrigued by the Morrison (1975) paper, and when it became apparent that there was enough time remaining in the visibility period for a few of our stars to allow observations in this region after our primary observations were complete, we availed ourselves of this opportunity (see Sec. 2.2.2). We did not use these lines to determine the model fits previously described; instead, we simply use the near-UV observations here to set the stage for future work, by comparing with our model fits.

We have data in the near-UV for two of the stars in this paper, AV 26 and LH101:W3-24. The first of these is an O6 I(f) supergiant, and the latter an O3 V((f)) dwarf. Neither has He II $\lambda4686$ in emission, however. The spectrum of AV 26 has a good SNR (100 per 2-pixel spectral resolution element), while the spectrum of LH101:W3-24 is much noisier (SNR=11 per 2-pixel spectral resolution element).

We show the spectra and the model predictions in Fig. 25. First, we note that neither star has measurable He I $\lambda3187$ in its spectrum. The adopted model for AV 26 predicts a slightly stronger He I $\lambda3187$ than observed, while the agreement for LH101:W3-24 is as good as the signal-to-noise allows. Second, the He II $\lambda3203$ line is very well matched for AV 26. The synthetic He II $\lambda3203$ spectrum may not be strong enough in LH101:W3-24; it is hard to tell, given the poor SNR. Further comparisons are planned in the next paper in this series.

5. Conclusions and Summary

We have attempted to model the spectra of 20 O-type stars in the Magellanic Clouds, succeeding in obtaining adequate or good fits in 17 cases. We suspect that the other three stars are binaries, and expect that a few more in our sample are in reality composite spectra, given the statistical expectations that a third of (Galactic) O-type stars are spectroscopic binaries. The physical parameters of the stars which were successfully modeled are well determined, and should permit us to refine the effective temperature scale.

In describing the spectral features in our sample, we were struck by the fact that several of our SMC stars appear to be more luminous than their "f" characteristics (N III $\lambda4634, 42$ and He II $\lambda4686$) would indicate. Although one cannot rule out a binary explanation, we did not see such discrepancies amoung our LMC sample. N III emission is a complex NLTE effect, while He II $\lambda4686$ is formed in the stellar wind and will be affected by the mass-loss rates, although in a manner that can not be predicted with any certainty by theory at this time, as under different physical conditions one might expect that the He II emission is either weaker or stronger at low metallicities. One would not, however, expect *a priori* that these "f" characteristics would exhibit the *same* behavior at low metallicity as they do in Galactic objects. We have identified here several examples where the He II emission is weaker than one might expect given the star's M_V, while the referee Nolan Walborn has kindly reminded us of two additional examples in the SMC, Sk 80 and AV 83, where the He II $\lambda4686$ emission is possibly *stronger* than in many Galactic counterparts. More modeling of both Galactic and SMC stars are needed to understand this issue.

In the second paper of this series we will roughly double the sample of Magellanic Cloud stars that have been analyzed in this manner. However, it is tempting to compare the effective temperatures we have derived here with those recently found for Galactic stars by Repolust et al. (2004). We show this comparison in Fig. 26, where we have separated the effective temperatures by luminosity class. For comparison, we also show the effective temperature scales determined by Conti (1988) (dashed line) and Vacca et al. (1996).

The data for the giants are too sparse as yet to draw any conclusions. However, for both the dwarfs and the supergiants we see that the Magellanic Cloud stars have *significantly* higher temperatures than their Galactic counterparts in the range from the earliest types through mid-O. By the late O-types, there is less of a difference. The data are also too sparse yet to draw firm conclusions about differences in the effective temperature scales for O stars for the SMC vs. LMC. In the sample we have analyzed so-far we have mainly very early O-type stars in the LMC, and somewhat later types in the SMC. We will be able to address this more fully in the second paper in this series, where we complete our Magellanic Cloud sample.

Nevertheless, this result is quite intriguing. As described in Sec. 1, we would expect the lower mass-loss rates (due to the lower metallicities) in the Clouds to result in a higher effective temperature in comparison to a star of the same spectral subtype in the Milky Way: first, there will be less wind emission affecting the He I. In addition, the smaller metallicity will lead to reduced *wind-blanketing* and *line-blanketing*. Together, these combine to result in effective temperatures which are $\sim 3000 - 4000°K$ (10%) greater at O5 V for the Magellanic Cloud stars in our sample.

We note with some irony that despite the substantial improvements in the stellar models over the years, the older effective temperature scales of Conti (1973) and Conti (1988), based primarily on the original non-LTE models of Auer & Mihalas (1972), have held up remarkably well for the Galactic stars. Work over the next few years will result in an improved scale that will take metallicity into account, but for now the Conti (1988) scale is to be preferred over more recent editions (e.g., Vacca et al. 1996).

Three recent studies have analyzed a limited sample of Magellanic Cloud O stars using CMFGEN. Crowther et al. (2002) studied 4 extreme O supergiants (luminosity class "Iaf+") in the Clouds, and derived temperatures that are considerably lower than those shown in Fig. 26a for our sample. Hillier et al. (2003) analyzed the SMC stars extreme supergiant Az 83 (O7 Iaf+) and Az 69 (OC7.5 III((f))). The supergiant is also cooler than what we find, but this may be due to the fact that the more extreme supergiants have lower effective temperatures. The giant star agrees well with the Galactic giants. Bouret et al. (2003) have examined the spectra of five O dwarfs and one O-type giant in the NGC 346 cluster in the SMC. Here the results are more mixed. The temperature of the star they classify as an O2 III is in accord with what we find (Fig. 25b), as are some of the results for the dwarfs. Others of their dwarfs have effective temperatures lower than what Repolust et al. (2004) found for Galactic stars of the same spectral type. Are the differences due to the different models being employed? We withhold any judgement until a similar sized sample of stars have been analyzed with both codes.

In the second paper in this series we will complete our Magellanic Cloud sample. At that time, we will also examine the effect that the new data have on the wind-momentum luminosity relation, and give a comparison between the masses derived from the present atmosphere fits and those of stellar evolutionary models.

REFERENCES

Abbott, D. C., & Hummer, D. G. 1985, ApJ, 294, 286

Ardeberg, A. & Maurice, E. 1977, A&AS, 30, 261

Asplund, M. 2003, in CNO in the Universe, ed. C. Harbonnel, D. Schaerer, & G. Meynet (San Francisco: ASP), 275

Auer, L. H., & Mihalas, D. 1972, ApJS, 24, 193

Azzopardi, M, & Vigneau, J. 1982, A&AS, 50, 291

Bianchi, L., & Garcia, M. 2002, ApJ, 581, 610

Bouret, J.-C., Lanz, T., Hillier, D. J., Heap, S. R., Hubeny, I., Lennon, D. J., Smith, L. J., & Evans, C. J. 2003, ApJ, 595, 1182

Bresolin, F., Kudritzki, R.-P., Lennon, D. J., Smartt, S. J., Herrero, A., Urbaneja, M.A., & Puls, J. 2002, ApJ, 580, 213

Cameron, A. G. W. 1982, in Essays in Nuclear Astrophysics, ed. C. A. Barnes, D. D. Clayton, & D. N. Schramm (Cambridge: Cambridge Univ. Press), 23

Conti, P. S. 1973, ApJ, 179, 181

Conti, P. S. 1988, in O Stars and Wolf-Rayet Stars, ed. P. S. Conti & A. B. Underhill (Washington, D. C.: NASA SP-497), 129

Conti, P. S., & Alschuler, W. R. 1971, ApJ, 170, 325

Crampton, D. C., & Greasley, J., 1982, PASP, 94, 31

Crowther, P. A., Hillier, D. J., Evans, C. J., Fullerton, A. W., De Marco, O., & Willis, A. J. 2002, ApJ, 579, 774

de Koter, A., Heap, S. R., & Hubeny, I. 1997, ApJ, 477, 792

de Koter, A., Heap, S. R., & Hubeny, I. 1998, ApJ, 509, 879

Gabler, R., Gabler, A., Kudritzki, R. P., Puls, J., & Pauldrach, A. 1989, A&A, 226, 162

Garmany, C. D., Conti, P. S., & Massey, P. 1980, ApJ, 242, 1063

Garmany, C. D., Conti, P. S., & Massey, P. 1987, AJ, 93, 1070

Garnett, D. R. 1999, in New Views of the Magellanic Clouds, IAU Symp. 190, ed. Y.-H. Chu, N. Suntzeff, J. Hesser, & D. Bohlender (San Francisco, ASP), 266

Haser, S. M. 1995, Ph.D. thesis, Univ.-Sternwarte der Ludwig-Maximilian Univ., Muenchen

Haser, S. M., Lennon, D. J., Kudritzki, R.-P., Puls, J., Pauldrach, A. W. A., Bianchi, L., & Hutchings, J. B. 1995, A&A, 295, 136

Herrero, A., Kudritzki, R. P., Vilchez, J. M., Kunze, D., Butler, K., & Haser, S. 1992, A&A, 261, 209

Herrero, A., Puls, J., Corral, L. J., Kudritzki, R.-P., & Villamariz, M. R. 2001, A&A, 366, 623

Herrero, A., Puls, J., & Najarro, F. 2002, A&A, 396, 949

Hillier, D., Lanz, T., Heap, S. R., Hubeny, I., Smith, L. J., Evans, C. J., Lennon, D. J., & Bouret, J. C. 2003, ApJ, 588, 1039

Hillier, D., & Miller, D. L. 1998, ApJ, 496, 407

Horne, K. 1988, in New Directions in Spectrophotometry, ed. A. G. D. Philips, D. S. Hayes, & S. J. Adelman (Schenectady: L. Davi Press), 285

Hummer, D. G. 1982, ApJ, 257, 724

Hunter, D. A., Vacca, W. D., Massey, P., Lynds, R., & O'Neil, E. J. 1997, AJ, 113, 1691

Jaschek, C., & Jaschek, M. 1990, The Classification of Stars (Cambridge: Cambridge Univ. Press), 136

Johnson, H. L., & Morgan, W. W. 1953, ApJ, 117, 313

Klein, R. I., & Castor, J. I. 1978, ApJ, 220, 902

Kubat, J., Puls, J., & Pauldrach, A. W. A. 1999, A&A, 341, 587

Kudritzki, R. P. 1975, Astron. Gesellschaft, Mitteilungen, 36, 81

Kudritzki, R. P. 1976, A&A, 52, 11

Kudritzki, R. P. 1980, A&A, 85, 174

Kudritzki, R. P. 1991, in Stellar Atmospheres: Beyond Classical Models, Proceedings of the Advanced Research Workshop, 174

Kudritzki, R. P., Cabanne, M. L., Husfeld, D., Niemela, V. S., Groth, H. G., Puls, J., & Herrero, A. 1989, A&A, 226, 235

Kudritzki, R. P., & Hummer, D. G. 1990, ARA&A, 28, 303

Kudritzki, R. P, & Puls, J. 2000, ARA&A, 38, 613

Kudritzki, R. P., Simon, K. P., & Hamann, W.-R. 1983, A&A, 121, 85

Kurucz, R. L. 1992, in The Stellar Populations of Galaxies, ed. B. Barbuy & A. Renzini (Dodrecht, Kluwer), 225

Lamers, H. J. G. L. M., Cerruti-Sola, M., & Perinotto, M. 1987, ApJ, 314, 726

Leitherer, C., Leão, J. R. S., Heckman, T. M., Lennon, D. J., Pettini, M., & Robert, C. 2001, ApJ, 550, 724

Lennon, D. J., Becker, S. T., Butler, K., Eber, F., Groth, H. G., Hunze, D., & Kudritzki, R.-P. 1991, A&A, 252, 498

Lucke, P. 1972, PhD Thesis, Univ. Washington

Maeder, A., & Meynet, G. 2000, ARA&A, 38, 143

Malumuth, E. M., & Heap, S. R. 1994, AJ, 107, 1054

Martins, F., Schaerer, D., & Hillier, D. J. 2002, A&A, 382, 999

Massey, P. 1998a, in The Stellar Initial Mass Function, 38th Herstmonceux Conference, ed. G. Gilmore & D. Howell (San Francisco: ASP), 17

Massey, P. 1998b, in Stellar Astrophysics for the Local Group, ed. A. Aparicio, A. Herrero, & F. Sanchez (Cambridge: Cambridge Univ. Press), 95

Massey, P. 2002, ApJS, 141, 81

Massey, P. 2003, ARA&A, 41, 15

Massey, P., & Hunter, D. A. 1998, ApJ, 493, 180

Massey, P., & Olsen, K. A. G. 2003, AJ, 126, 2867

Massey, P., Penny, L. R., & Vukovich, J. 2002, ApJ, 565, 982

Massey, P., Waterhouse, E., & DeGioia-Eastwood, K. 2000, AJ, 119, 2214

Mihalas, D. 1978, Stellar Atmospheres, 2nd Edition (San Francisco: Freeman),

Mihalas, D., & Hummer, D. G. 1973, ApJ, 179, 827

Morrison, N. D. 1975, ApJ, 202, 433

Oey, M. S., & Kennicutt, R. C., Jr. 1997, MNRAS, 291, 827

Pauldrach, A. W. A., Hoffmann, T. L., & Lennon, M. 2001, A&A, 375, 161

Prinja, R. K., & Crowther, P. A. 1996, A&A, 311, 264

Puls, J., Kudritzki, R.-P., Herrero, A., Pauldrach, A. W. A., Haser, S. M., Lennon, D. J., Gabler, R., Voels, S. A., Vilchez, J. M., Wachter, S., & Feldmeier, A. 1996, A&A, 305, 171

Repolust, T., Puls, J., & Herrero, A. 2004, A&A, in 415, 349

Robert, C. 1999, in Wolf-Rayet Phenomena in Massive Stars and Starburst Galaxies, ed. K. A. van der Hucht, G. Koenigsberger, & P. R. J. Eeenens (San Francisco: ASP), 616

Russell, S. C., & Dopita, M. A. 1990, ApJS, 74, 93

Santolaya-Rey, A. E., Puls, J., & Herrero, A. 1997 A&A, 323, 488

Schaerer, D., Meynet, G., Maeder, A., & Schaller, G. 1993, A&AS, 98, 523

Schaerer, D. & Schmutz, W. 1994, A&A, 288, 231

Sellmaier, F., Puls, J., Kudritzki, R. P., Gabler, A., Gabler, R., & Voels, S. A. 1993, A&A, 273, 533

Shaver, P. A., McGee, R. X., Newton, L. M., Danks, A. C., & Pottasch, S. R. 1983, MNRAS, 204, 53

Simon, K. P., Kudritzki, R. P., Jonas, G., & Rahe, J. 1983, A&A, 125, 34

Smith, L. J., Norris, R. P. F., & Crowther, P. A. 2002,

Taresch, G., Kudritzki, R. P., Hurwitz, M., Bowyer, S., Pauldrach, A. W. A., Puls, J., Butler, K., Lennon, D. J., & Haser, S. M. 1997, A&A, 321, 531

Testor, G., & Niemela, V. 1998, A&AS, 130, 527

Urbaneja, M. A., Herrero, A., Kudritzki, R.-P., Bresolin, F., Corral, L. J., & Puls, J. 2002, A&A, 386, 1019

Vacca, W. D., Garmany, C. D., & Shull, J. M. 1996, ApJ, 460, 914

Valdes, F. 1992, in Astronomical Data Analysis Software and Systems I, (San Francisco: ASP), 398

van den Bergh, S. 2000, The Galaxies of the Local Group (Cambridge: Cambridge Univ. Press)

Voels, S. A., Bohannan, B., Abbott, D. C. 1989, ApJ, 340, 1073

Walborn, N. R. 1971a, ApJS, 23, 257

Walborn, N. R. 1971b, ApJ, 167, L31

Walborn, N. R., & Fitzpatrick, E. L. 1990, PASP, 102, 379

Walborn, N. R., Fullerton, A. W., Crowther, P. A., Bianchi, L., Huitchings, J. B., Pellerin, A., Sonneborn, G., &Willis, A. J. 2002b, ApJS, 141, 443

Walborn, N. R., Howarth, I. D., Lennon, D. J., Massey, P., Oey, M. S., Moffat, A. F. J., Skalkowski, G., Morrell, N. I., Drissen, L., & Parker, J. W. 2002a, AJ, 123, 2754

Walborn, N. R., Lennon, D. J., Heap, S. R., Lindler, D. J., Smith, L. J., Evans, C. J., & Parker, J. W. 2000, PASP, 112, 1243

Walborn, N. R., Morrell, N. I., Howarth, I. D., Crowther, P. A., Lennon, D. J., Massey, P., & Arias, J. I. 2004, ApJ, submitted

Weigelt, G., & Baier, G. 1985, A&A, 150, L18

Westerlund, B. E. 1961, Uppsala Astron. Obs. Ann., 5, 1

Westerlund, B. E. 1997, The Magellanic Clouds (Cambridge: Cambridge Univ. Press)

Table 1.   Program Stars[a]

Name[b]	Cat ID[c]	α_{2000}	δ_{2000}	V	$B-V$	$U-B$	$E(B-V)$[d]	M_V[e]	Spectral Type[f]
AV 14	SMC-007187	00 46 32.57	-73 06 05.4	13.55	-0.17	-1.00	0.15	-5.8	O5 V
AV 26	SMC-009337	00 47 49.99	-73 08 20.7	12.46	-0.17	-1.00	0.16	-7.0	O6 I(f)
AV 75	SMC-016828	00 50 32.39	-72 52 36.1	12.70	-0.15	-1.00	0.20	-6.9	O5.5 I(f+)
AV 207	SMC-043724	00 58 33.20	-71 55 46.8	14.25	-0.20	-1.06	0.11	-5.0	O7.5 V((f))
AV 296	SMC-052948	01 02 08.57	-72 13 19.9	14.26	-0.19	-1.02	0.13	-5.1	O7.5 V((f))
AV 372	SMC-055537	01 03 10.49	-72 02 14.2	13.03	-0.16	-1.04	0.15	-6.8	O9.5 I
AV 377	SMC-061105	01 05 07.42	-72 48 18.1	14.45	-0.20	-1.06	0.14	-4.9	O5 V((f))
AV 378	SMC-061202	01 05 09.39	-72 05 34.7	13.77	-0.20	-1.02	0.12	-5.5	O9.5 III
AV 396	SMC-063226	01 06 04.25	-72 13 34.2	14.10	-0.19	-1.00	0.12	-5.2	B0 III
AV 451	SMC-071002	01 10 26.06	-72 23 28.9	13.97	-0.22	-1.04	0.07	-5.2	O9.5 III
AV 469	SMC-073337	01 12 28.97	-72 29 29.2	13.12	-0.16	-1.05	0.13	-6.2	O8.5 I(f)
LH64-16=LH64:W16-8	LMC-142269	05 28 46.97	-68 47 47.9	13.61	-0.22	-1.11	0.11	-5.2	ON2 III(f*)[g]
LH81:W28-5[h]	$\cdots$	05 34 28.47	-69 43 56.6	13.92	-0.18	-1.10	0.15	-5.0	O4 V((f+))
LH101:W3-24=ST5-27[i]	$\cdots$	05 39 14.10	-69 30 03.8	14.58	-0.10	-1.00	0.25	-4.7	O3 V((f))
R136-020=R136a5[j]	$\cdots$	05 38 42.5208	-69 06 03.112	13.93	$\cdots$	$\cdots$	0.42	-6.0	O2 If*
R136-024=R136a7[j]	$\cdots$	05 38 42.4992	-69 06 02.961	14.06	$\cdots$	$\cdots$	0.41	-5.8	O3 III(f*)
R136-036=R136a-608[j]	$\cdots$	05 38 42.7584	-69 06 03.214	14.49	$\cdots$	$\cdots$	0.46	-5.5	O2 If*[k]
R136-040=R136a-535[j]	$\cdots$	05 38 42.5555	-69 06 01.587	14.60	$\cdots$	$\cdots$	0.38	-5,2	O3 V
R136-047=R136a-602[j]	$\cdots$	05 38 42.7331	-69 06 03.658	14.68	$\cdots$	$\cdots$	0.46	-5.3	O2 III(f*)
R136-055=R136a-551[j]	$\cdots$	05 38 42.5984	-69 06 04.977	14.86	$\cdots$	$\cdots$	0.40	-5.0	O3 V

[a]Coordinates and photometry are from Massey 2002, unless otherwise noted.

[b]Identifications are as follows: "AV" from Azzopardi & Vigneau 1982; "LH" from Lucke 1972, "W" from Westerlund 1961; "ST" from Testor & Niemela 1998; "R136-NNN" from Hunter et al. 1997 and Massey & Hunter 1998; "R136aN" from Weigelt & Baier 1985, "R136a-NNN" from Malumuth & Heap 1994.

[c]Designations from the catalog of Massey 2002.

[d]From averaging the color excesses in $B-V$ and $U-B$ based upon the spectral type. See Massey 1998b.

[e]Computed using $A_V = 3.1 \times E(B-V)$, with assumed distance moduli for the SMC and LMC of 18.9 and 18.5, respectively (Westerlund 1997, van den Bergh 2000). The M_V values for the R136 stars were taken from Massey & Hunter 1998.

[f]New to this paper.

[g]Classified as O2 III(f*) by Walborn et al. 2002, and reclassifed as ON2 III(f*) by Walborn et al. 2004.

[h]Coordinates and photometry from Massey, Waterhouse, & DeGioia-Eastwood 2000.

[i]Coordinates and photometry from Testor & Niemela 1998.

[j]Coordinates and photometry from Hunter et al. 1997 and Massey & Hunter 1998. Although UBV photometry has been published by Malumuth & Heap 1994, this was based upon pre-COSTAR imaging; comparison with V from the post-COSTAR data of Hunter et al. 1997 shows poor agreement.

[k]Classified as O2-O3 If* by Walborn et al. 2002, who refer to the star as "MH 36"

Table 2.   Data Used In This Study

Star	Telescope	Instrument	Observer	Date year-month-day	Aperture (arcsec x arcsec)	Grating	Wavelength (Å)	Resolution (Å)	Exp. time (sec)
UV									
AV 14	HST/5444	FOS	Robert	1994-09-24	3.7x3.7	G130H	1140-1600	1.0	480
AV 26	HST/5444	FOS	Robert	1995-03-11	3.7x3.7	G130H	1140-1600	1.0	480
AV 26	HST/9012	STIS	Massey	2002-07-31	0.2x0.2	G140L	1150-1740	0.9	445
AV 75	HST/5444	FOS	Robert	1995-01-18	3.7x3.7	G130H	1140-1600	1.0	480
AV 207	HST/5444	FOS	Robert	1994-10-21	3.7x3.7	G130H	1140-1600	1.0	480
AV 296	HST/8633	STIS	Massey	2000-09-02	0.2x0.2	G140L	1150-1740	0.9	210
AV 372	HST/5444	FOS	Robert	1994-11-16	3.7x3.7	G130H	1140-1600	1.0	480
AV 377	HST/5444	FOS	Robert	1995-11-02	3.7x3.7	G130H	1140-1600	1.0	480
AV 378	HST/5444	FOS	Robert	1995-03-08	3.7x3.7	G130H	1140-1600	1.0	480
AV 396	HST/5444	FOS	Robert	1995-01-29	3.7x3.7	G130H	1140-1600	1.0	480
AV 451	HST/5444	FOS	Robert	1995-03-11	3.7x3.7	G130H	1140-1600	1.0	480
AV 469	HST/5444	FOS	Robert	1995-03-09	3.7x3.7	G130H	1140-1600	1.0	480
LH64-16	HST/8633	STIS	Massey	2001-01-01	0.2x0.2	G140L	1150-1740	0.9	150
LH81:W28-5	HST/8633	STIS	Massey	2000-11-13	0.2x0.2	G140L	1150-1740	0.9	120
LH101:W3-24	HST/8633	STIS	Massey	2001-01-31	0.2x0.2	G140L	1150-1740	0.9	360
R136-020	HST/5297	GHRS	Heap	1994-04-03	0.2x0.2	G140L	1160-1450	0.6	1792
R136-020	HST/5297	GHRS	Heap	1994-04-02	0.2x0.2	G140L	1460-1750	0.6	7168
R136-024	HST/6018	GHRS	Heap	1996-02-03	0.2x0.2	G140L	1160-1450	0.6	1795
R136-024	HST/6018	GHRS	Heap	1996-02-03	0.2x0.2	G140L	1460-1750	0.6	3590
R136-036	HST/6018	GHRS	Heap	1996-02-02	0.2x0.2	G140L	1160-1450	0.6	2992
R136-036	HST/6018	GHRS	Heap	1996-02-02	0.2x0.2	G140L	1460-1750	0.6	5984
R136-040	HST/6018	GHRS	Heap	1996-02-03	0.2x0.2	G140L	1160-1450	0.6	3617
R136-040	HST/6018	GHRS	Heap	1996-02-03	0.2x0.2	G140L	1460-1750	0.6	7181
R136-047	HST/6018	GHRS	Heap	1996-02-01	0.2x0.2	G140L	1160-1450	0.6	4189
R136-047	HST/6018	GHRS	Heap	1996-02-01	0.2x0.2	G140L	1460-1750	0.6	7779
R136-055	HST/6018	GHRS	Heap	1996-02-02	0.2x0.2	G140L	1160-1450	0.6	9792
R136-055	HST/6018	GHRS	Heap	1996-02-02	0.2x0.2	G140L	1460-1750	0.6	4189
$H\alpha$									
AV14	CTIO 4-m	RC	Massey	1999-01-06	1.3x330	KPGLD	5400-7800	2.8	600
AV26	CTIO 4-m	RC	Massey	1999-01-06	1.3x330	KPGLD	5400-7800	2.8	300
AV26	HST/9412	STIS	Massey	2002-07-31	0.2x52	G750M	6300-6850	0.8	360
AV75	CTIO 4-m	RC	Massey	1999-01-06	1.3x330	KPGLD	5400-7800	2.8	300
AV207	CTIO 4-m	RC	Massey	1999-01-06	1.3x330	KPGLD	5400-7800	2.8	376
AV296	CTIO 4-m	RC	Massey	1999-01-06	1.3x330	KPGLD	5400-7800	2.8	900
AV372	CTIO 4-m	RC	Massey	1999-01-06	1.3x330	KPGLD	5400-7800	2.8	300
AV377	CTIO 4-m	RC	Massey	1999-01-06	1.3x330	KPGLD	5400-7800	2.8	1200
AV469	CTIO 4-m	RC	Massey	1999-01-06	1.3x330	KPGLD	5400-7800	2.8	300
LH64-16	CTIO 4-m	RC	Massey	1999-01-06	1.3x330	KPGLD	5400-7800	2.8	600
LH81:W28-5	CTIO 4-m	RC	Massey	1999-01-06	1.3x330	KPGLD	5400-7800	2.8	600
LH101:W3-24	HST/9412	STIS	Massey	2002-05-30	0.2x52	G750M	6300-6850	0.8	1800
R136-020	HST/7739	STIS	Massey	1998-02-04	0.2x52	G750M	6300-6850	0.8	280
R136-024	HST/7739	STIS	Massey	1998-02-03	0.2x52	G750M	6300-6850	0.8	370
R136-036	HST/7739	STIS	Massey	1998-02-04	0.2x52	G750M	6300-6850	0.8	490

Table 2—Continued

Star	Telescope	Instrument	Observer	Date year-month-day	Aperture (arcsec x arcsec)	Grating	Wavelength (Å)	Resolution (Å)	Exp. time (sec)
R136-040	HST/7739	STIS	Massey	1998-02-04	0.2x52	G750M	6300-6850	0.8	280
R136-047	HST/7739	STIS	Massey	1998-02-05	0.2x52	G750M	6300-6850	0.8	660
R136-055	HST/7739	STIS	Massey	1998-02-03	0.2x52	G750M	6300-6850	0.8	775
Blue									
AV14	CTIO 4-m	RC	Massey	1999-01-03	1.3x330	KPGLD	3750-4900	1.4	900
AV26	CTIO 4-m	RC	Massey	1999-01-04	1.3x330	KPGLD	3750-4900	1.4	600
AV75	CTIO 4-m	RC	Massey	1999-01-05	1.3x330	KPGLD	3750-4900	1.4	900
AV207	CTIO 4-m	RC	Massey	1999-01-04	1.3x330	KPGLD	3750-4900	1.4	600
AV296	CTIO 4-m	RC	Massey	1999-01-05	1.3x330	KPGLD	3750-4900	1.4	900
AV372	CTIO 4-m	RC	Massey	1999-01-05	1.3x330	KPGLD	3750-4900	1.4	300
AV377	CTIO 4-m	RC	Massey	1999-01-04	1.3x330	KPGLD	3750-4900	1.4	600
AV378	CTIO 4-m	RC	Massey	1999-01-04	1.3x330	KPGLD	3750-4900	1.4	747
AV396	CTIO 4-m	RC	Massey	1999-01-05	1.3x330	KPGLD	3750-4900	1.4	600
AV451	CTIO 4-m	RC	Massey	1999-01-04	1.3x330	KPGLD	3750-4900	1.4	600
AV469	CTIO 4-m	RC	Massey	1999-01-05	1.3x330	KPGLD	3750-4900	1.4	600
LH64-16	CTIO 4-m	RC	Massey	1999-01-04	1.3x330	KPGLD	3750-4900	1.4	1200
LH81:W28-5	CTIO 4-m	RC	Massey	1999-01-07	1.3x330	KPGLD	3750-4900	1.4	300
LH101:W3-24	CTIO 4-m	RC	Massey	1999-01-07	1.3x330	KPGLD	3750-4900	1.4	542
R136-020	HST/7739	STIS	Massey	1998-02-04	0.2x52	G430M	4310-4590	0.4	650
R136-020	HST/6417	FOS	Massey	1996-11-12	0.26(circ)	G400	3250-4820	3.0	770
R136-024	HST/7739	STIS	Massey	1998-02-03	0.2x52	G430M	4310-4590	0.4	825
R136-024	HST/6417	FOS	Massey	1996-11-12	0.26(circ)	G400	3250-4820	3.0	870
R136-036	HST/7739	STIS	Massey	1998-02-04	0.2x52	G430M	4310-4590	0.4	1150
R136-036	HST/6417	FOS	Massey	1996-11-13	0.26(circ)	G400	3250-4820	3.0	994
R136-040	HST/7739	STIS	Massey	1998-02-04	0.2x52	G430M	4310-4590	0.4	1330
R136-040	HST/6417	FOS	Massey	1997-01-01	0.26(circ)	G400	3250-4820	3.0	1042
R136-047	HST/7739	STIS	Massey	1998-02-05	0.2x52	G430M	4310-4590	0.4	1550
R136-047	HST/6417	FOS	Massey	1996-11-14	0.26(circ)	G400	3250-4820	3.0	1118
R136-055	HST/7739	STIS	Massey	1998-02-03	0.2x52	G430M	4310-4590	0.4	1750
R136-055	HST/6417	FOS	Massey	1996-11-14	0.26(circ)	G400	3250-4820	3.0	1180
Near-UV									
AV26	HST/9412	STIS	Massey	2002-07-31	0.2x52	G430M	3020-3300	0.4	250
LH101:W3-24	HST/9412	STIS	Massey	2002-05-30	0.2x52	G430M	3020-3300	0.4	200

Table 3.   Terminal Velocities in km s^{-1}

Star	v_∞	Comments[a]
AV 14	2000:	Weak emission
AV 26	2150	Second measurement: 2150
AV 75	2100	
AV 207	$\cdots$	No measurable wind
AV 296	2000	
AV 372	2000	C IV and Si IV
AV 377	2350::	From N V alone
AV 378	$\cdots$	No measurable wind
AV 396	$\cdots$	No measurable wind
AV 451	$\cdots$	No measurable wind
AV 469	2000	C IV and Si IV
LH64-16	3250	
LH81:W28-5	2700	
LH101:W3-24	2400	
R136-020	3400	dHH: 3000
R136-024	3100	P&C: $_{edge}$ =3135, dHH: 2900
R136-036	3700	P&C: 3640; dHH: 3750
R136-040	3400	P&C: 3000; dHH: 3400
R136-047	3500	P&C: 3305; dHH: 3625
R136-055	3250	P&C: 2955; dHH: 3150

[a]P&C=Prinja & Crowther 1998; dHH=de Koter, Heap, & Hubeny 1998

Table 4.   Results of Model Fits

Name	Spectral Type	$T_{\rm eff}$ (°K)	$\log g$ [cgs]	R ($R_\odot$)	M_V mags	BC mags	$M_{\rm bol}$ mags	Mass $M_\odot$	M-dot ($10^{-6} M_\odot$ yr^{-1})	β	v_∞ (km s^{-1})	He/H (by number)	Comments
AV 14	O5 V	44000	4.0	14.2	-5.8	-4.04	-9.8	74	0.1:	0.8	2000	0.10	$\dot{M} < 0.3$
AV 26	O6 I(f)	38000	3.5	27.5	-7.0	-3.63	-10.6	87	2.5	0.8	2150	0.10	
AV 75	O5.5 I(f)	40000	3.6	25.4	-6.9	-3.79	-10.7	94	3.5	0.8	2100	0.10	
AV 207	O7.5 V((f))	37000	3.7	11.0	-5.0	-3.53	-8.6	22	0.1:	0.8	2000	0.10	$\dot{M} < 0.3$
AV 296	O7.5 V((f))	35000	3.5	11.9	-5.1	-3.36	-8.5	16	0.5	0.8	2000	0.10	Poor fit. Binary?
AV 372	See Text	$\cdots$	$\cdots$	$\cdots$	-6.8	$\cdots$	$\cdots$	$\cdots$	$\cdots$	$\cdots$	2000	$\cdots$	Binary
AV 377	O5 V((f))	45500	4.0	9.1	-4.9	-4.14	-9.1	30	0.1:	0.8	2350	0.35	$\dot{M} < 0.3$; Strong NIII
AV 378	O9.5 III	31500	3.25	15.4	-5.5	-3.06	-8.6	15	(0.1)	(0.8)	(2000)	0.15	$\dot{M}$ not fit
AV 396	B0 III	30000	3.5	14.1	-5.2	-2.96	-8.2	23	(0.1)	(0.8)	(2000)	0.15	$\dot{M}$ not fit
AV 451	See Text	$\cdots$	$\cdots$	$\cdots$	-5.2	$\cdots$	$\cdots$	$\cdots$	$\cdots$	$\cdots$	$\cdots$	$\cdots$	Binary
AV 469	O8.5 I(f)	32000	3.1	21.2	-6.2	-3.12	-9.3	21	1.8	0.8	2000	0.20	
LH64-16	ON2 III(f*)	54500	3.9	9.4	-5.2	-4.67	-9.9	26	4.0	0.8	3250	1.0	See text
LH81:W28-5	O4 V((f+))	46000	3.8	9.6	-5.0	-4.17	-9.2	21	1.2	0.8	2700	0.20	
LH101:W3-24	O3 V((f))	48000	4.0	8.1	-4.7	-4.29	-9.0	24	0.5	0.8	2400	0.15	
R136-020	O2 If*	>42500	3.6	>16.4	-6.0	<-3.98	<-10.0	>39	23.0	0.8	3400	0.20	$T_{\rm eff}$ lower limit
R136-024	O3 III(f*)	$\cdots$	$\cdots$	$\cdots$	-5.8	$\cdots$	$\cdots$	$\cdots$	$\cdots$	$\cdots$	$\cdots$	$\cdots$	Binary
R136-036	O2 If*	>43000	3.7	>12.8	-5.5	<-4.00	<-9.5	>30	14.0	0.8	3700	0.10	$T_{\rm eff}$ lower limit
R136-040	O3 V	>51000	3.8	>10.3	-5.3	<-4.48	<-9.8	>24	2.0	0.8	3400	0.20	$T_{\rm eff}$ lower limit
R136-047	O2 III(f*)	>51000	3.9	>10.4	-5.3	<-4.49	<-9.8	>32	6.0	0.8	3500	0.10	$T_{\rm eff}$ lower limit
R136-055	O3 V	47500	3.8	9.4	-5.0	-4.26	-9.3	20	0.9	0.8	3250	0.10	
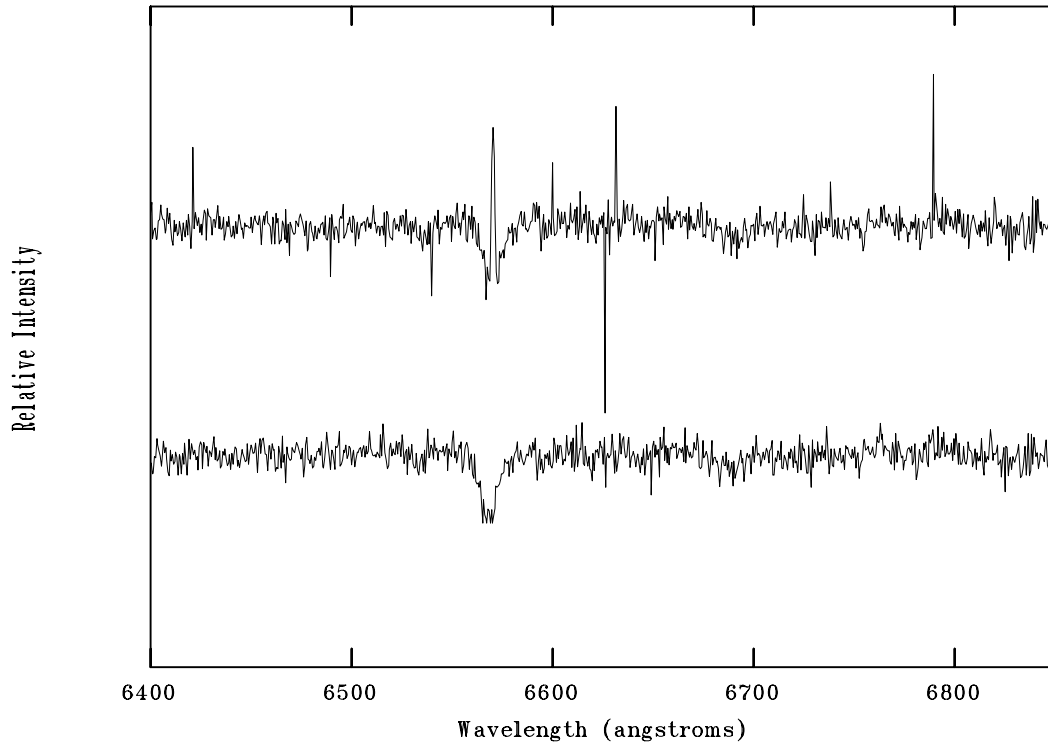
Fig. 1.— The difference between the standard CALSTIS pipeline reduction (upper) and the re-reduced spectrum with IRAF (lower) is shown for one of our program stars, LH101:W3-24. The data consist of a "CR-SPLIT" 300 sec exposure (i.e., two 150 sec segments) and are archived by STScI as data set "o6km14010). The complete Hα data set for this star consists of three such exposures. The SNR in the CALSTIS reduction is 18 in a spike-free region; the same region in the IRAF-reduced spectrum has a SNR of 22. The many spikes (due to cosmic rays and hot pixels) in the CALSTIS spectrum further degrade the SNR.

(a) R136–020

(b) R136–024

(c) R136–036

(d) R136–040
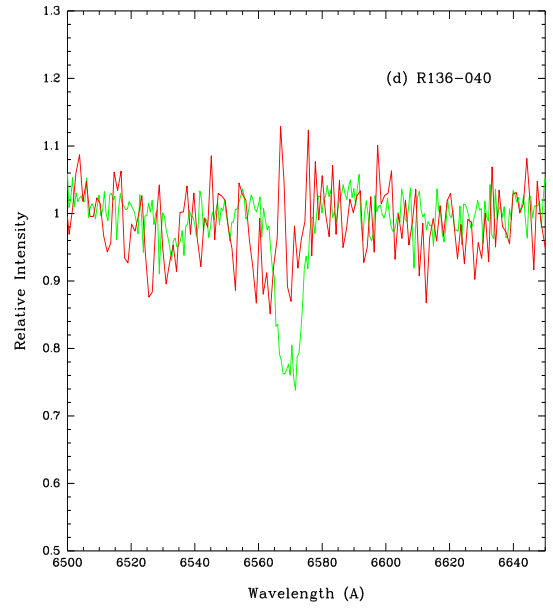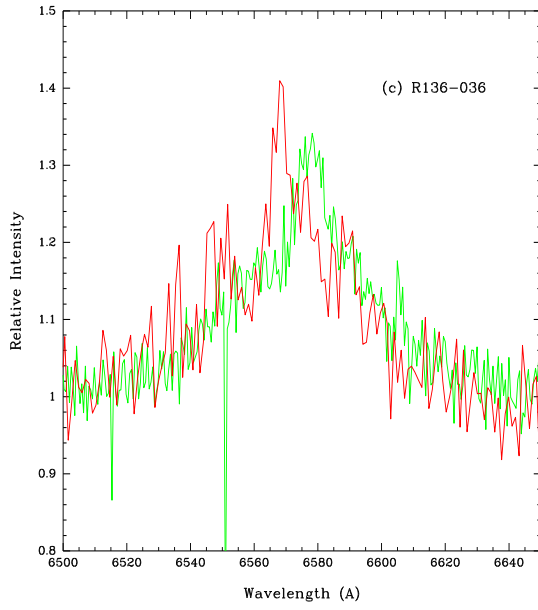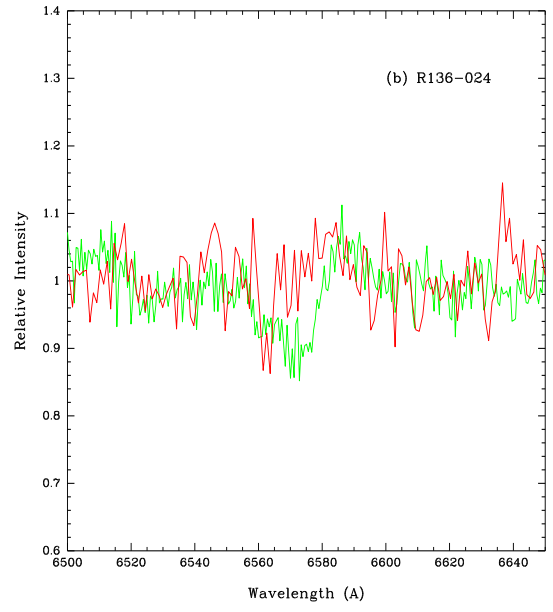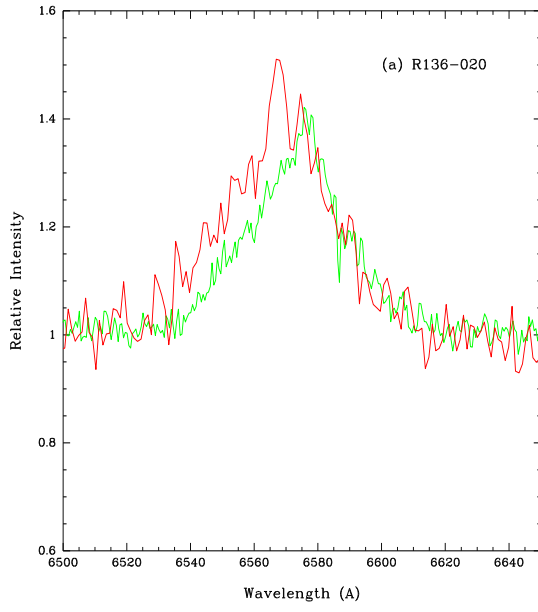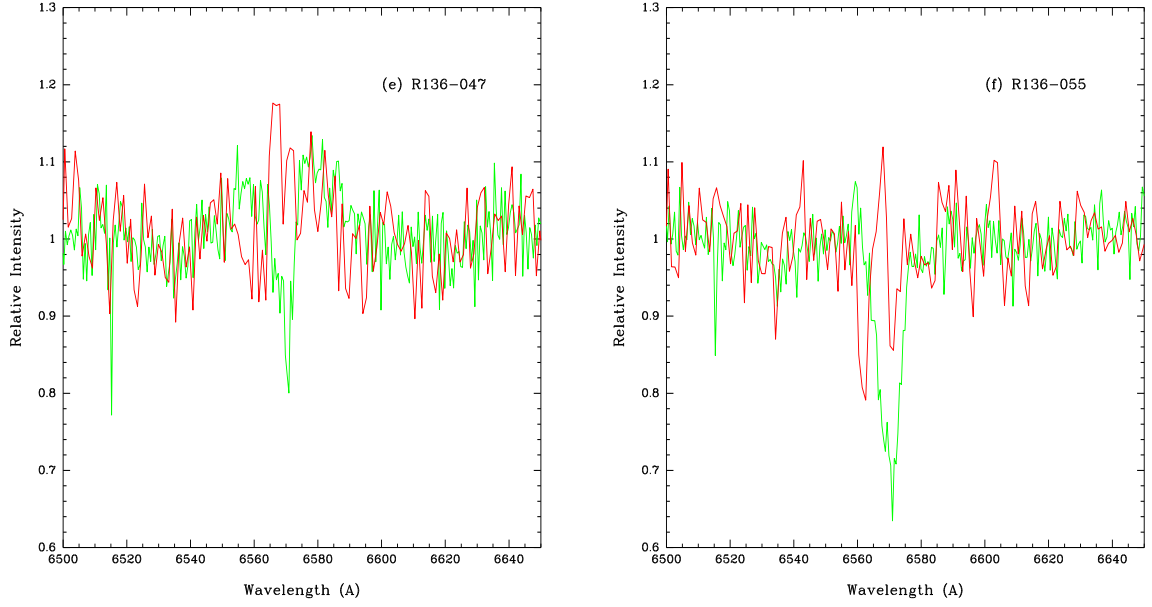
Fig. 2.— A comparison of our spectra (green) with the FOS spectra (red) used by de Koter et al. (1998) for the six R136 stars. In all cases there is additional emission present in the FOS data, due to nebular contamination.
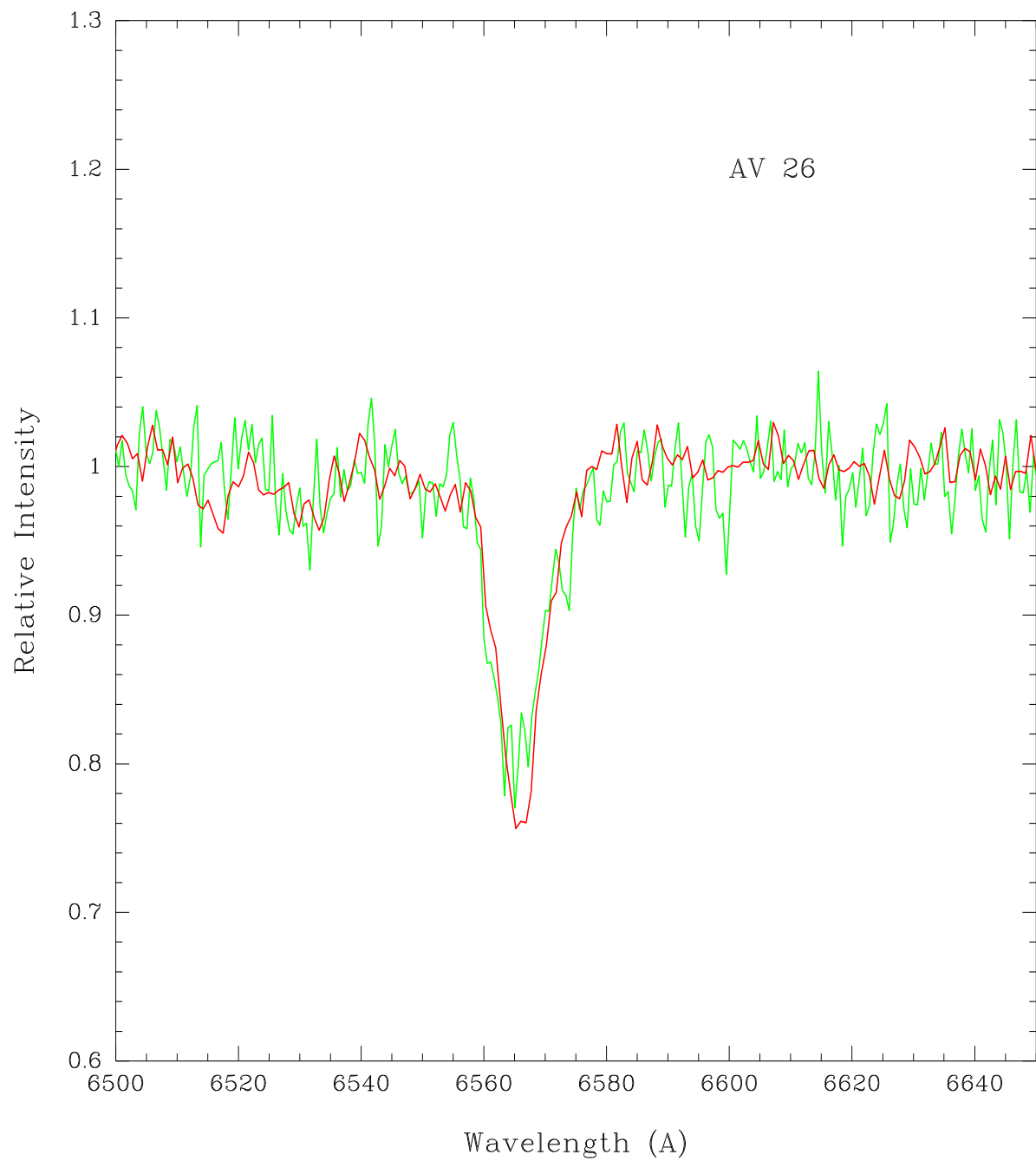
Fig. 3.— A comparison of our HST/STIS spectrum (green) with the ground-based CTIO spectra (red) of AV 26.
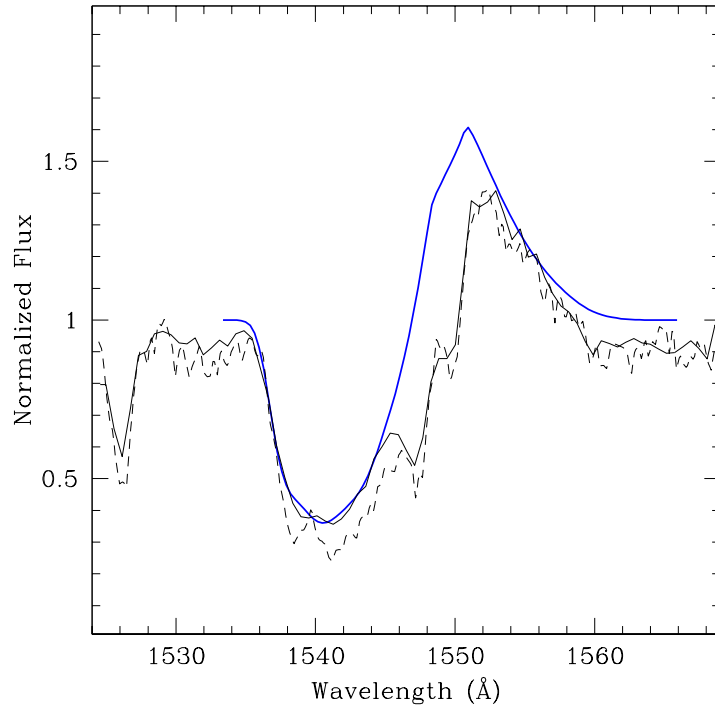
Fig. 4.— The two observations of the C IV $\lambda1550$ profile are shown by the solid (Cycle 12) and dashed (Cycle 9) black lines. Our fit is shown by the blue curve. The fact that the fit does not reproduce the absorption features on the longwards part of the profile and the emission peak is due to the fact that no correction for photospheric absorption has been made. This not not affect the determination of the terminal velocity.
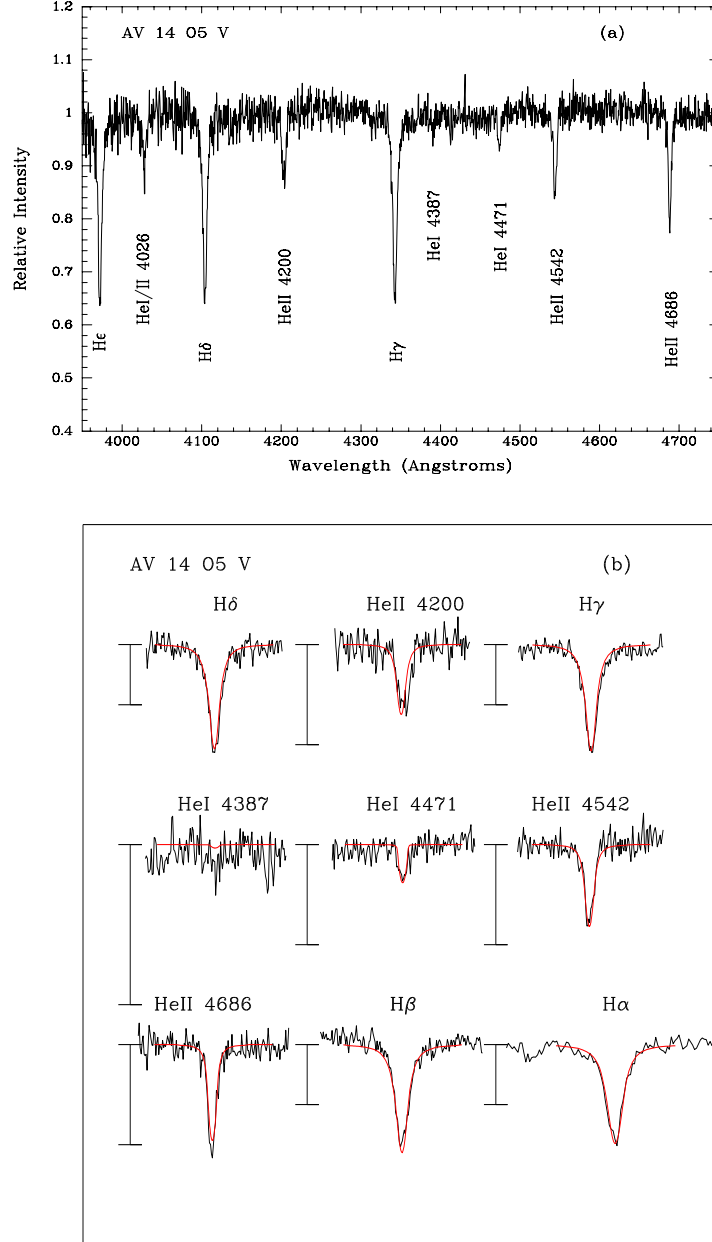
Fig. 5.— AV 14. (a) A portion of the blue-optical spectrum of AV 14 is shown with the major lines identified. (b) Selected spectral lines (black) are shown compared to the model fits (red). The bar to the left of each line shows a change of 20% intensity relative to the continuum, and the top of the bar denotes the continuum level. A radial velocity of 160 km s^{-1} and a rotational broadening $v \sin i$ of 150 km s^{-1} were used in making this comparison.
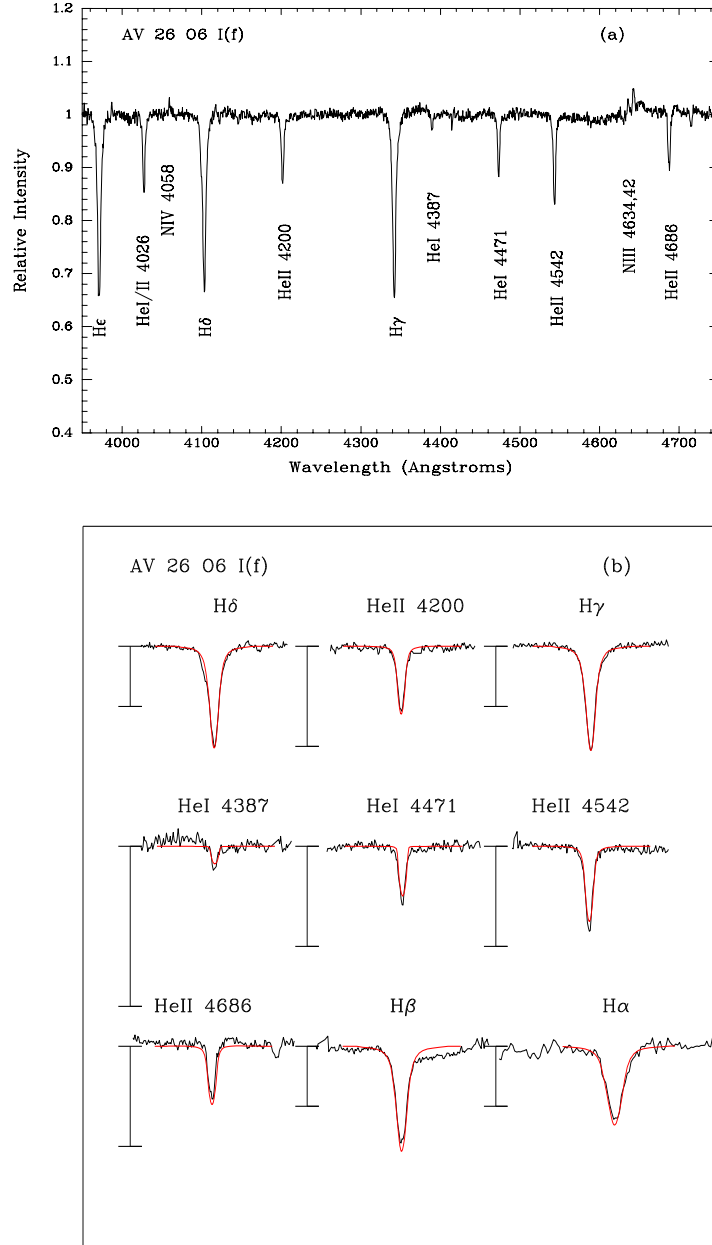
Fig. 6.— AV26. The same as Fig. 5, except that a radial velocity of 120 km s^{-1} and a rotational broadening $v \sin i$ of 150 km s^{-1} were used.
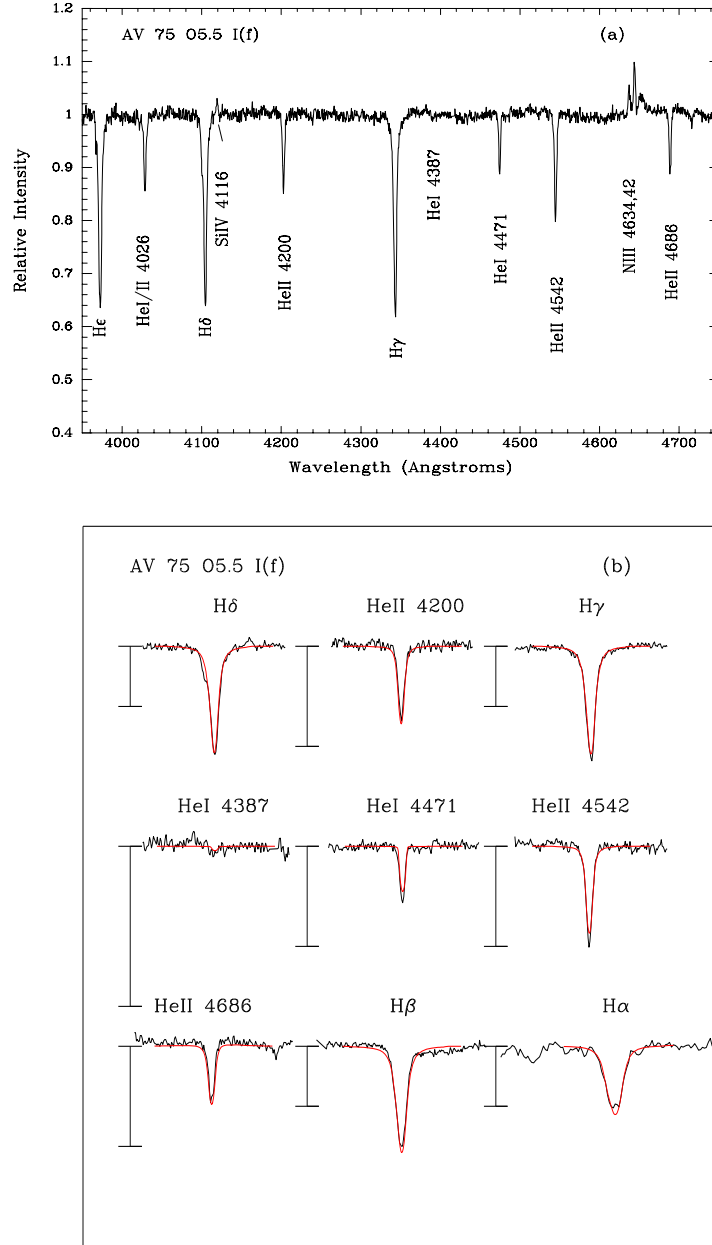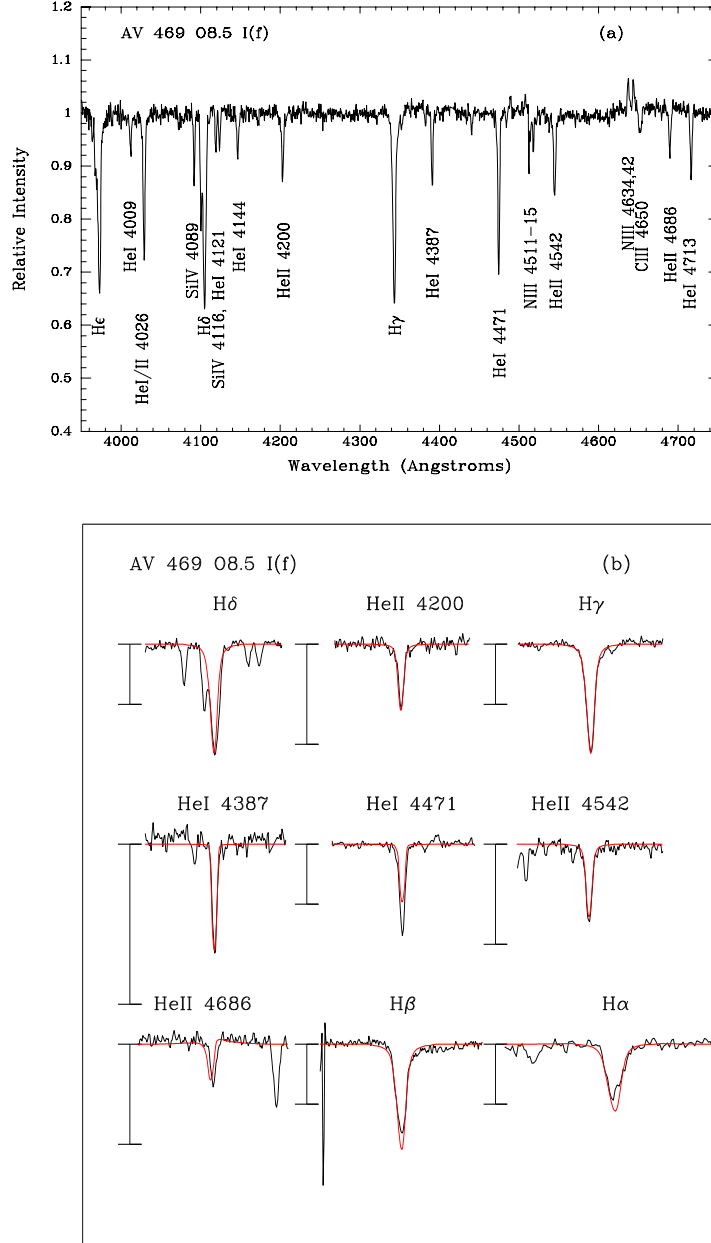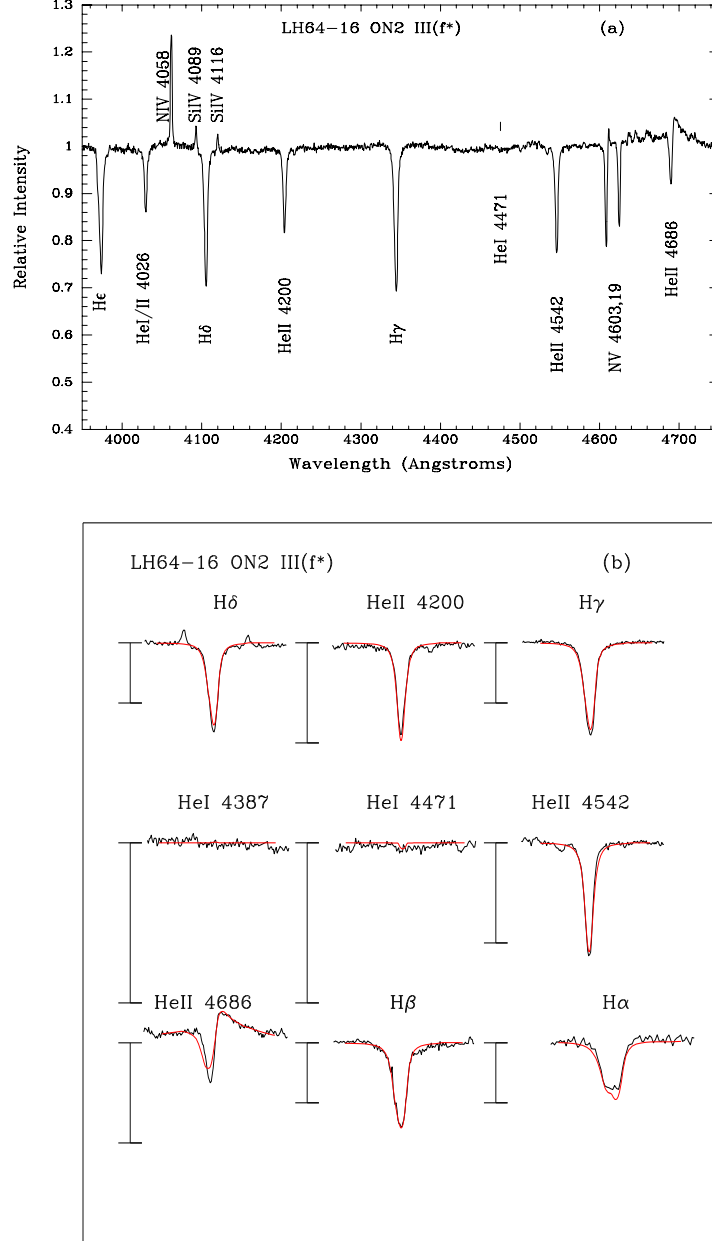
Fig. 7.— AV75. The same as Fig. 5, except that a radial velocity of 200 km s^{-1} and a rotational broadening of $v \sin i$ of 120 km s^{-1} have been adopted.
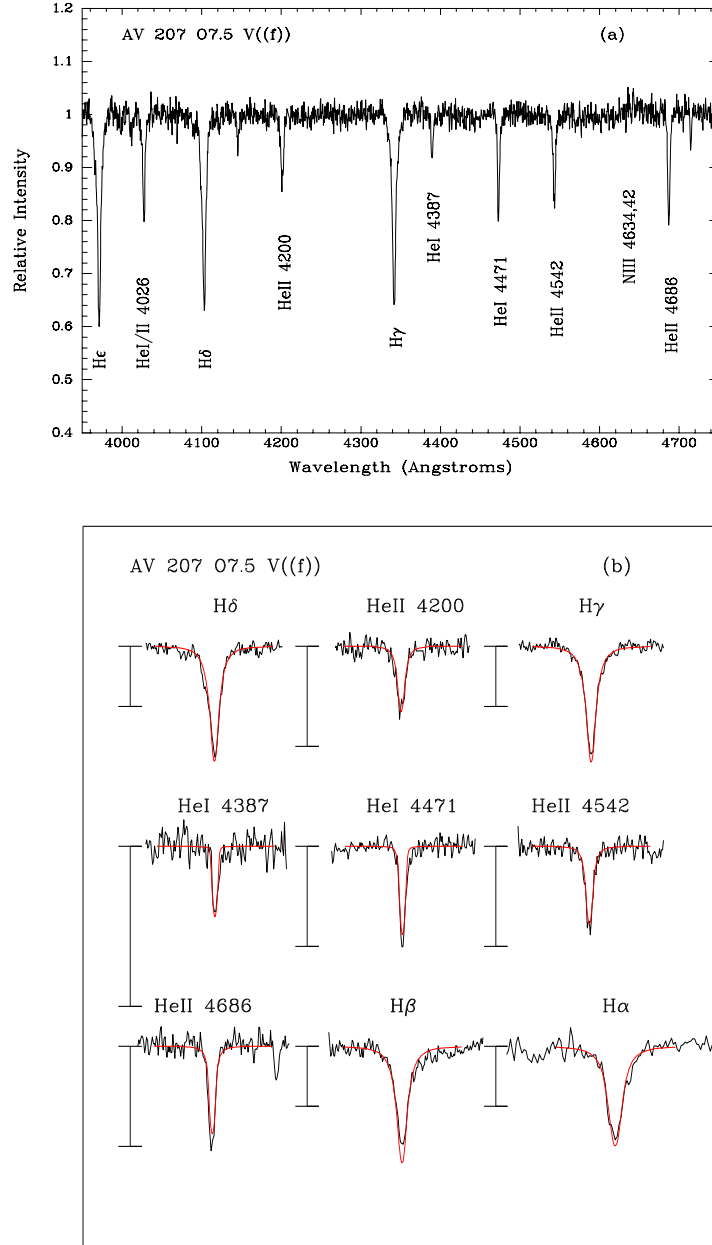
Fig. 8.— AV207. The same as Fig. 5, except that a radial velocity of 95 km s^{-1} and a rotational broadening of $v \sin i$ of 120 km s^{-1} have been adopted.
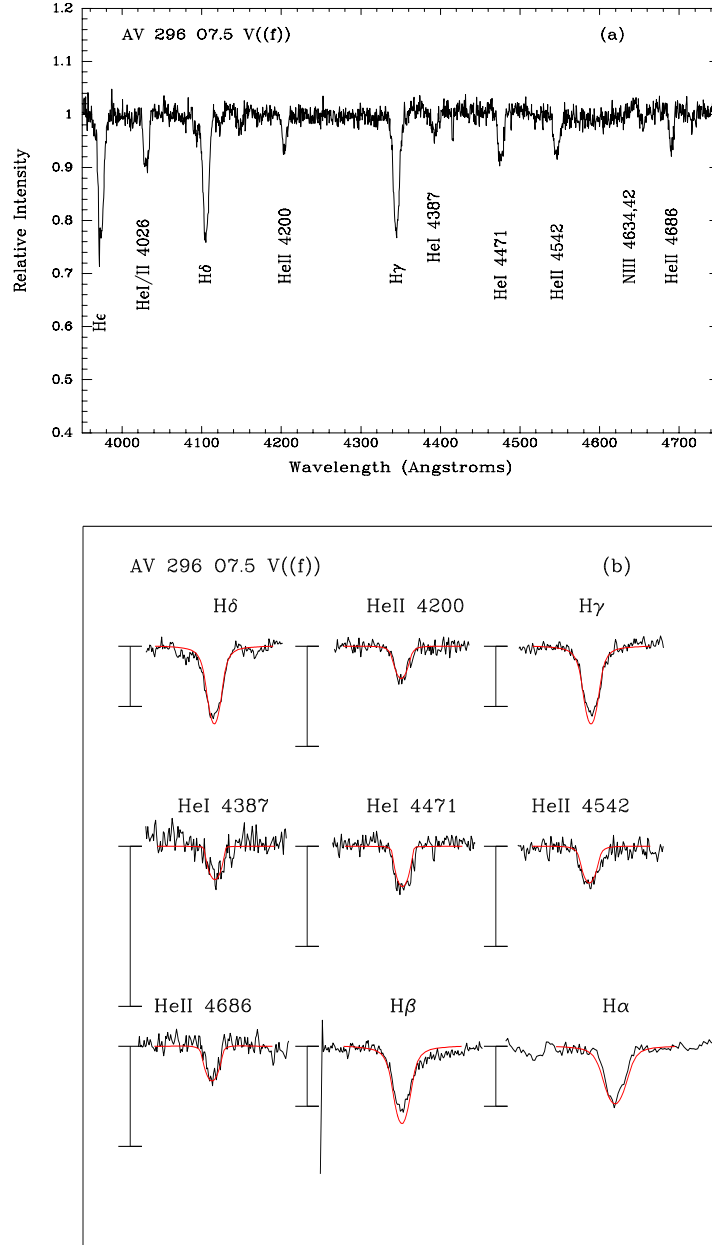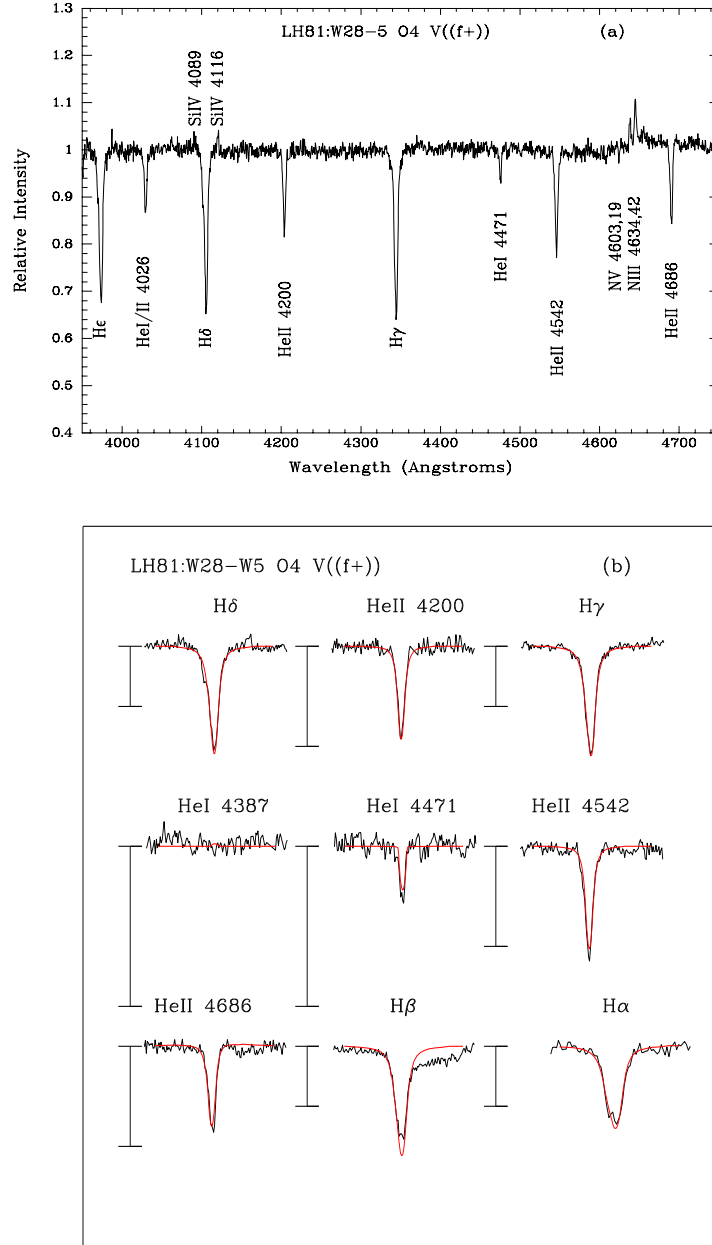
Fig. 9.— AV296. The same as Fig. 5, except that a radial velocity of 250 km s^{-1} and a rotational broadening of $v \sin i$ of 300 km s^{-1} have been adopted.
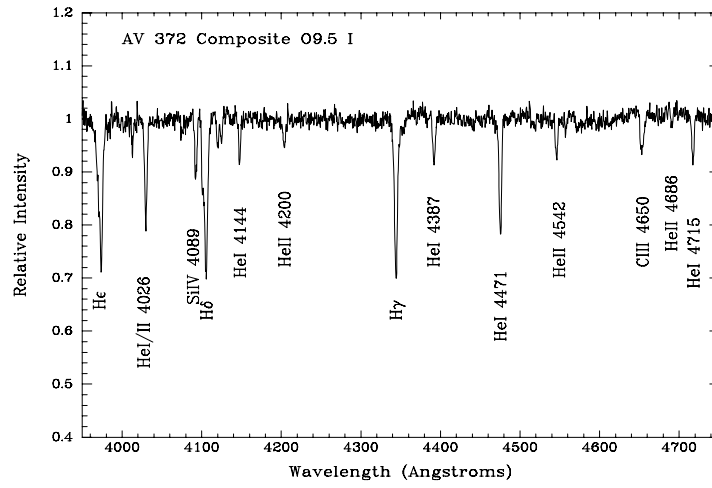
Fig. 10.— AV372. This star is likely a double-lined spectroscopic binary, with two stars contributing to the He I lines, and one star dominating the He II lines.
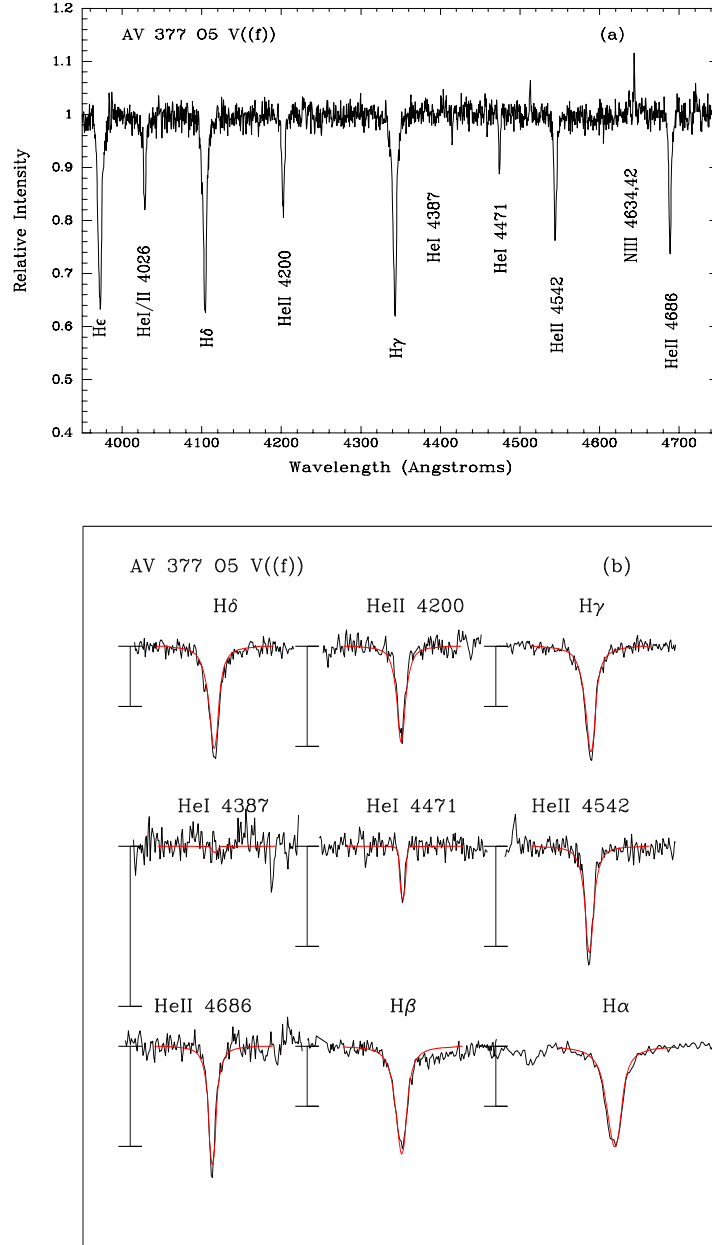
Fig. 11.— AV377. The same as Fig. 5, except that a radial velocity of 180 km s^{-1} and a rotational broadening of $v \sin i$ of 120 km s^{-1} have been adopted.
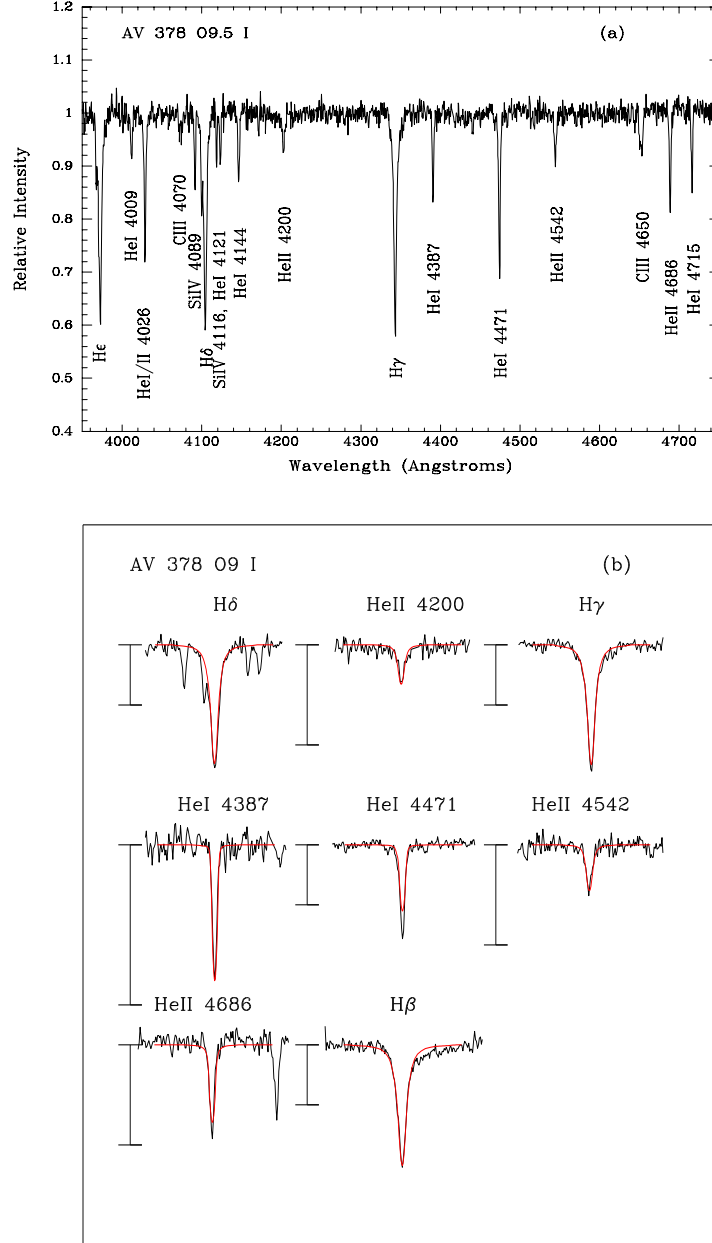
Fig. 12.— AV378. The same as Fig. 5, except that a radial velocity of 190 s^{-1} and a rotational broadening of $v \sin i$ of 110 km s^{-1} have been adopted. Note that the scale of He Iλ4471 has been changed with respect to earlier figures.
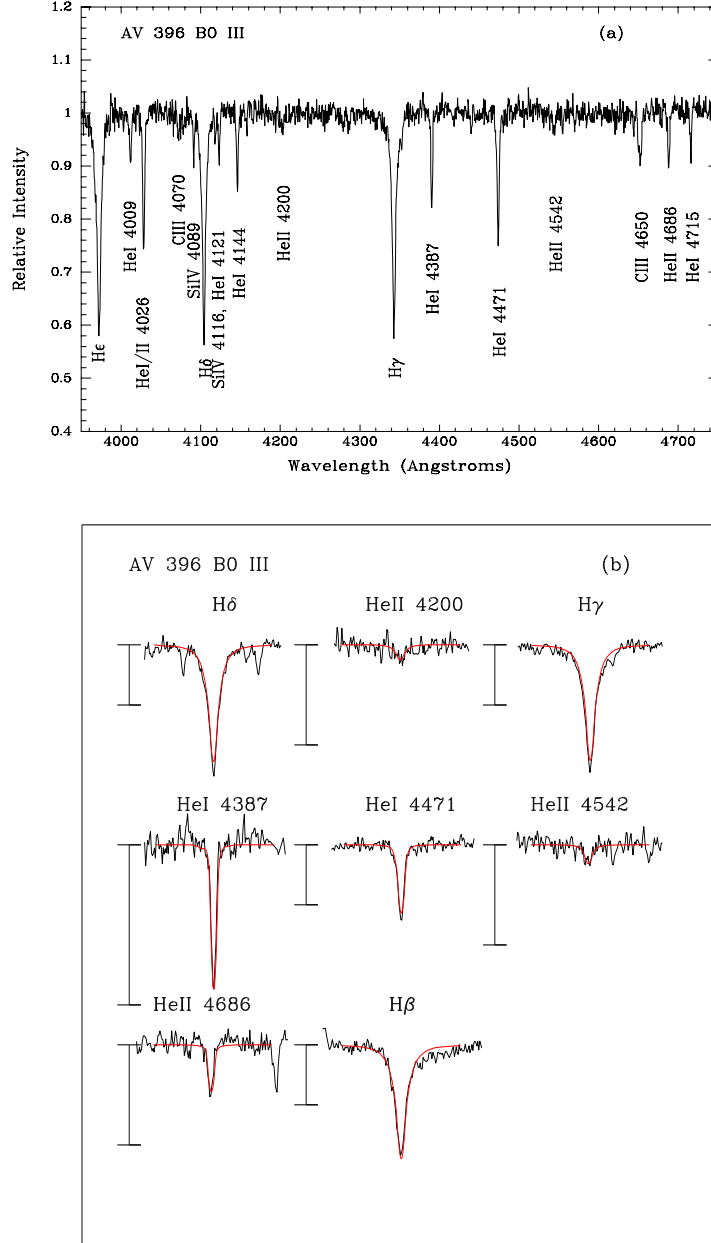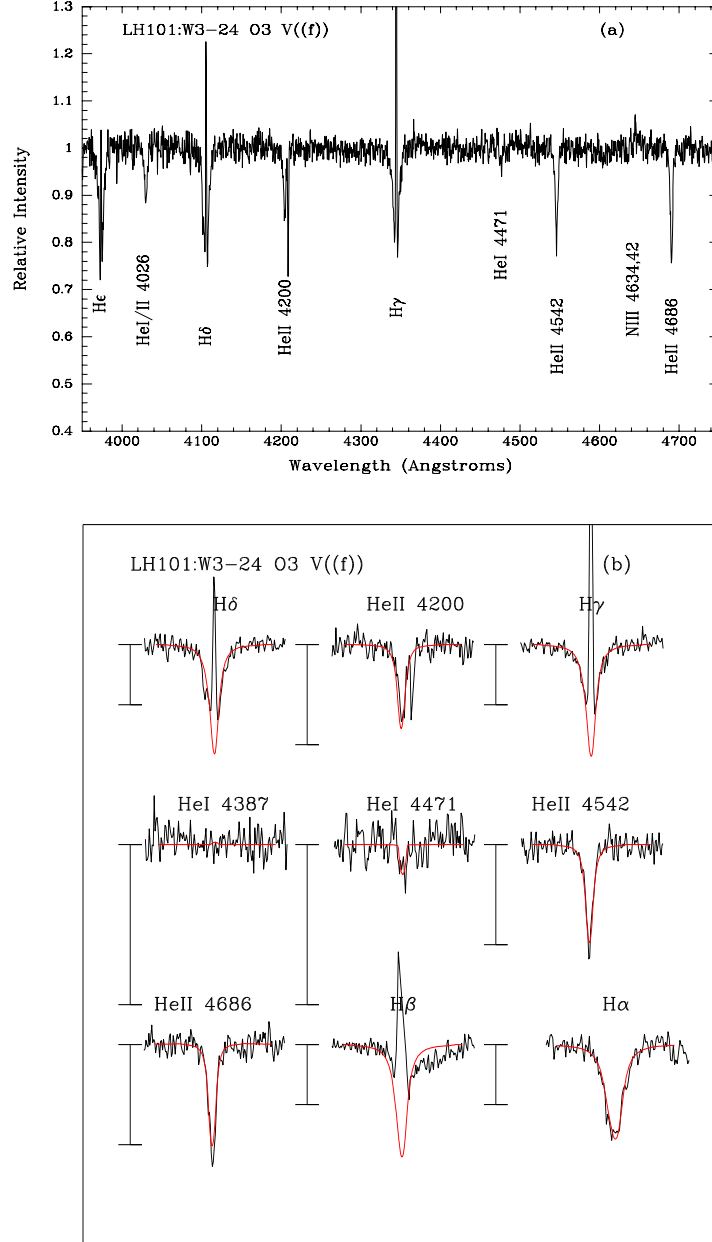
Fig. 13.— AV396. The same as Fig. 5, except that a radial velocity of 170 s⁻¹ and a rotational broadening of $v \sin i$ of 120 km s⁻¹ have been adopted. Note that the scale of He Iλ4471 has been changed with respect to Fig. 5.
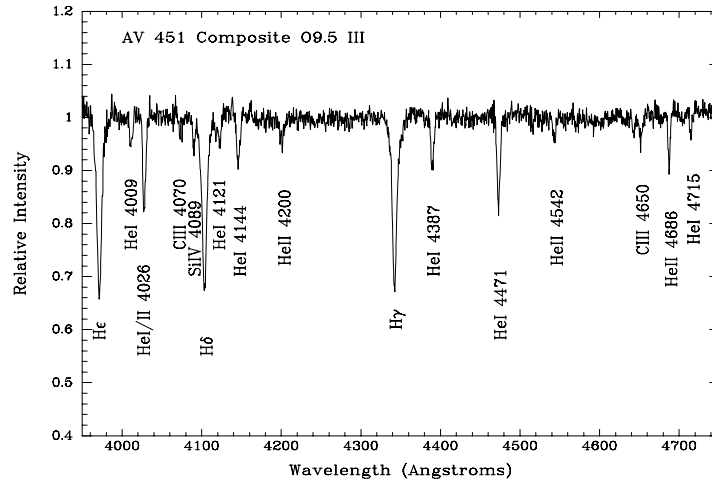
Fig. 14.— AV451. Like AV372 (Fig. 10), this star is judged to be an incipiently resolved double-lined binary, with two stars contributing He I, and one star dominating the He II contribution. The composite spectral type would be O9.5 III.

Fig. 15.— AV469. The same as Fig. 5, except that a radial velocity of 180 s^{-1} and a rotational broadening of $v \sin i$ of 110 km s^{-1} have been adopted. Note that the scale of He Iλ4471 has been changed with respect to Fig. 5.

Fig. 16.— LH64-16. The same as Fig. 5, except that a radial velocity of 290 s^{-1} and a rotational broadening of $v \sin i$ of 120 km s^{-1} have been adopted. The scale of He I $\lambda4471$ has now been magnified relative to that of earlier figures.

Fig. 17.— LH81:W28-5. The same as Fig. 5, except that a radial velocity of 280 s^{-1} and a rotational broadening of $v \sin i$ of 120 km s^{-1} have been adopted.

Fig. 18.— LH101:W3-24. The same as Fig. 5, except that a radial velocity of 280 s^{-1} and a rotational broadening of $v \sin i$ of 120 km s^{-1} have been adopted. Note that a cosmetic defect on the redward side of the He II λ4200 line, and the nebular emission at Hβ, have been suppressed in making this figure. The Hα profile is free of nebular contamination as it was obtained with *HST*'s superior spatial resolution.
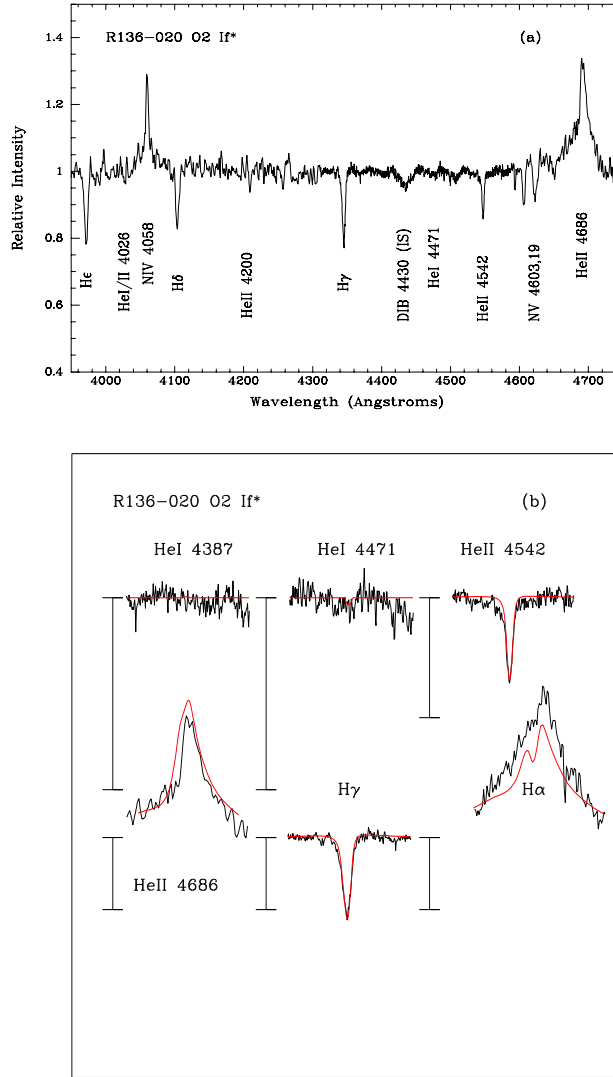
Fig. 19.— R136-020. In (a) we identify the major lines in the spectrum of R136-020. The data are from the FOS observations of Massey & Hunter (1998), except for the region 4310Å to 4590Å, where we have spliced in our higher SNR STIS spectrum. The relatively high interstellar extinction in the 30 Dor region results in the strong diffuse interstellar band (DIB) at λ4430. In (b) we show the match between the model spectra (red) and the observed spectrum (black). As in earlier figures, the bars denote a change in intensity of 20%, and the tops of the bars denote the continuum level. The He II λ4686 profile is from the FOS data; the rest are from STIS. A rotational velocity of 120 km s^{-1} has been adopted; uncertainties in the zero-point of the STIS wavelength scale prevent accurate radial velocity measurements.
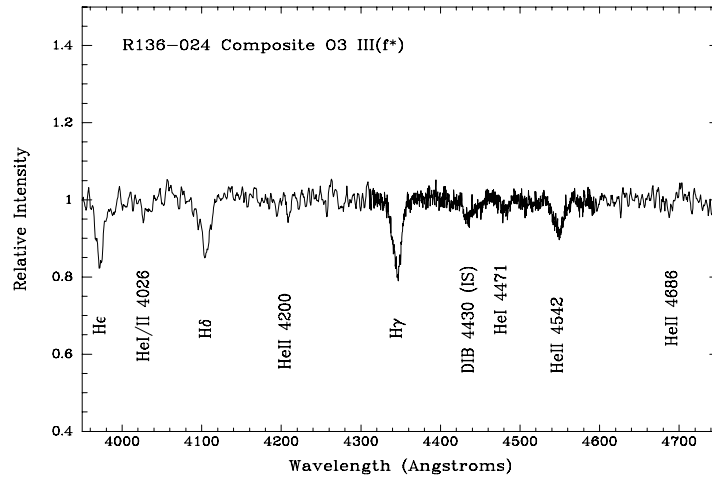
Fig. 20.— R136-024. The spectrum of R136-024 is likely a composite of two O3 V stars.
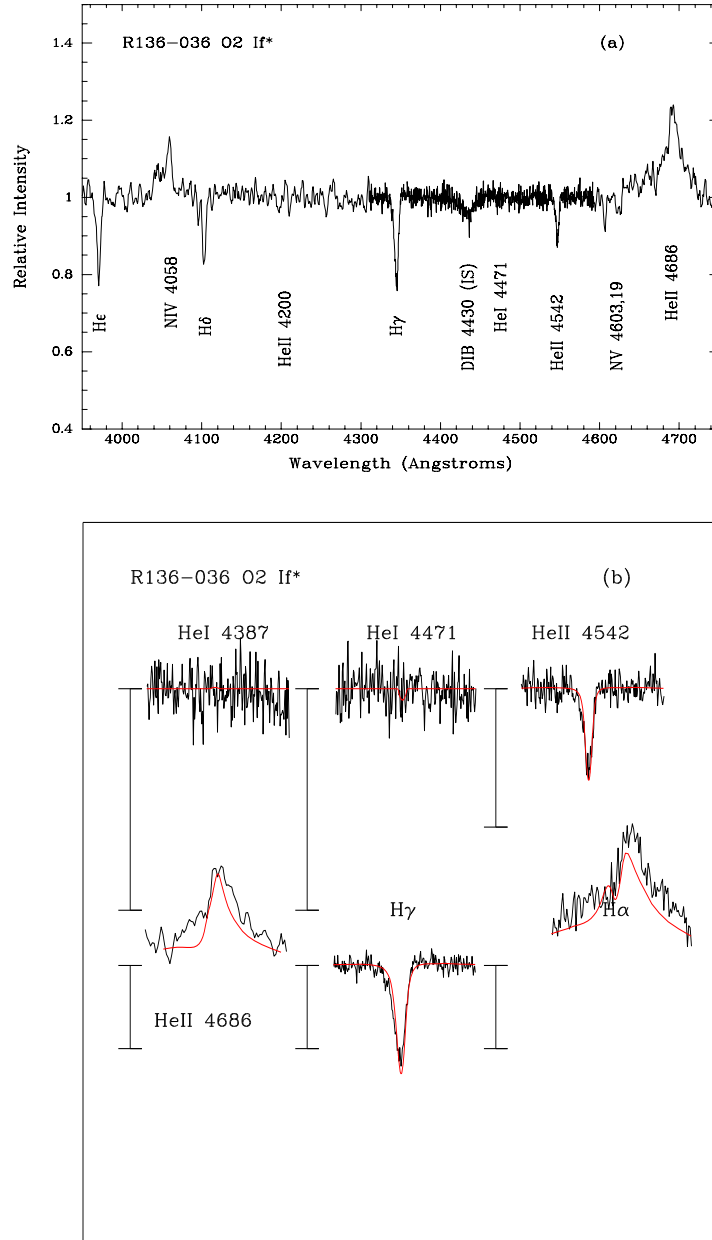
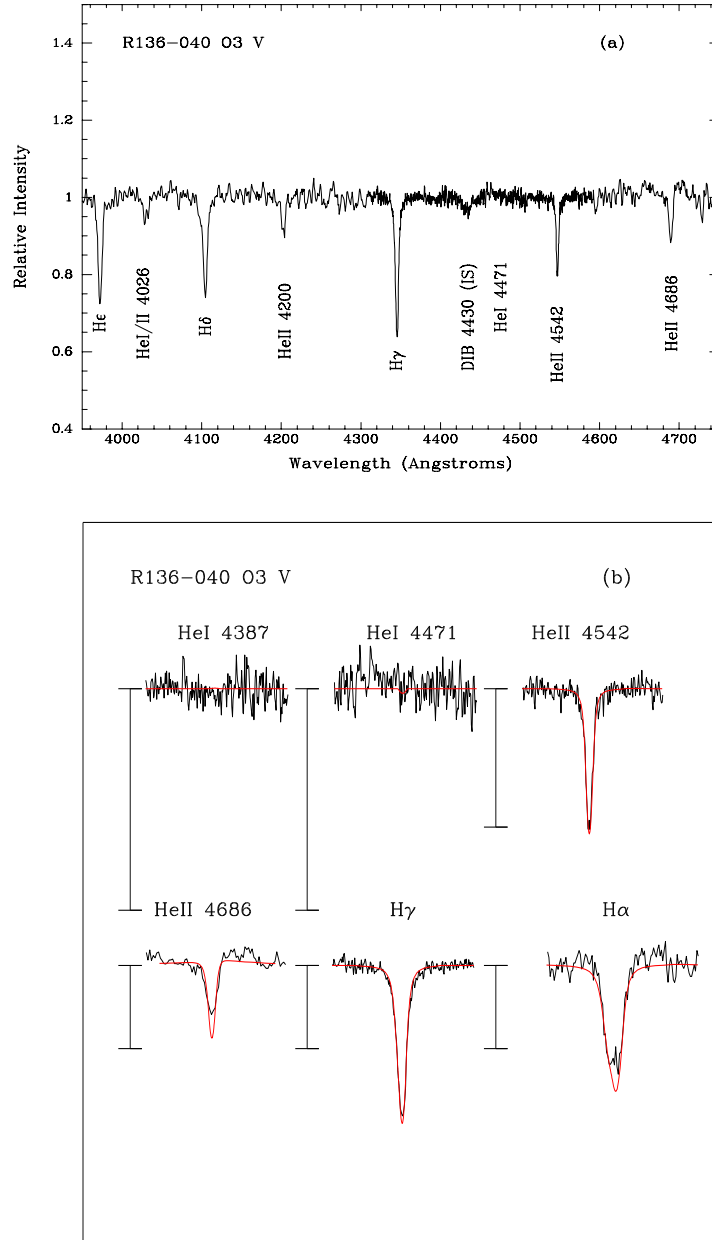Fig. 21.— R136-036. The same as Fig. 19.
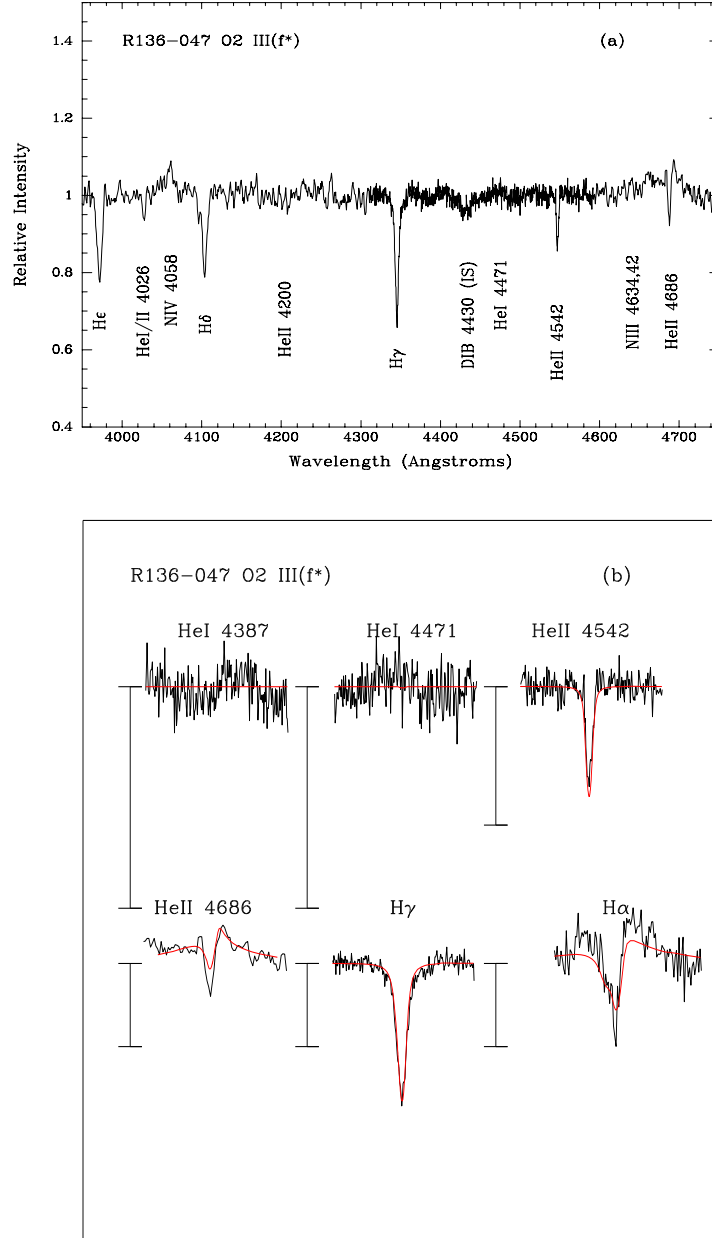
Fig. 22.— R136-040. The same as Fig. 19.
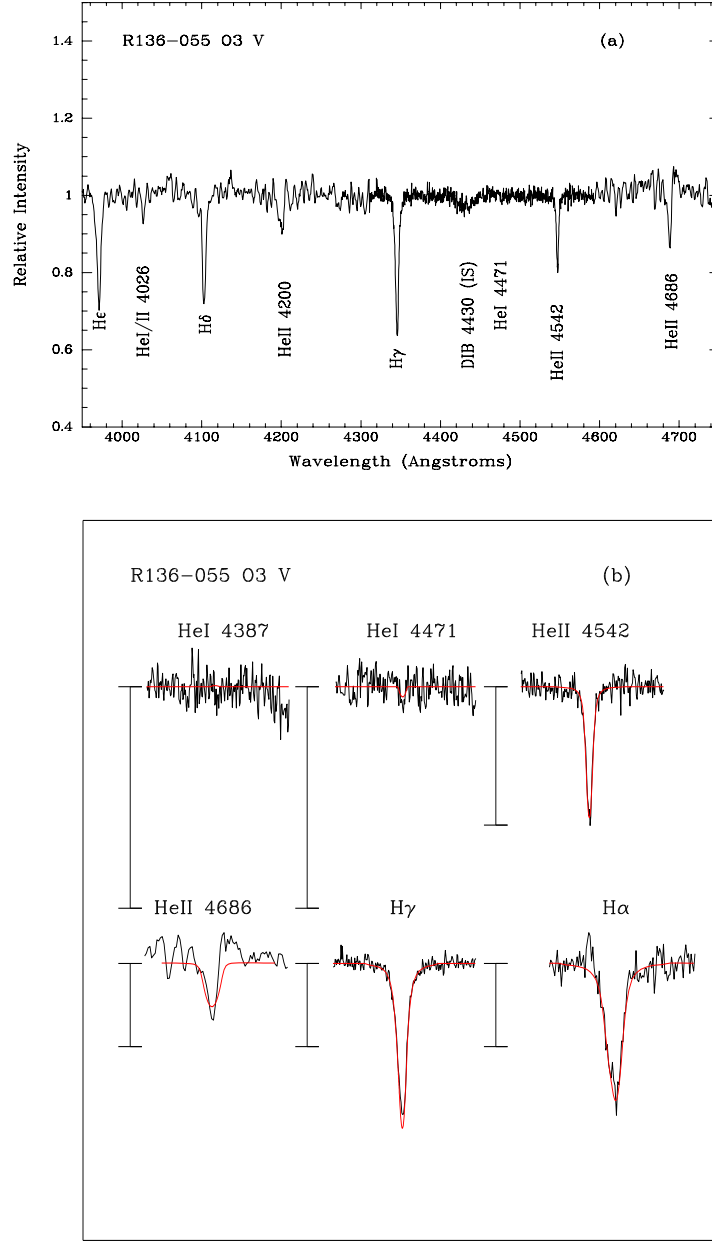
Fig. 23.— R136-047. The same as Fig. 19.
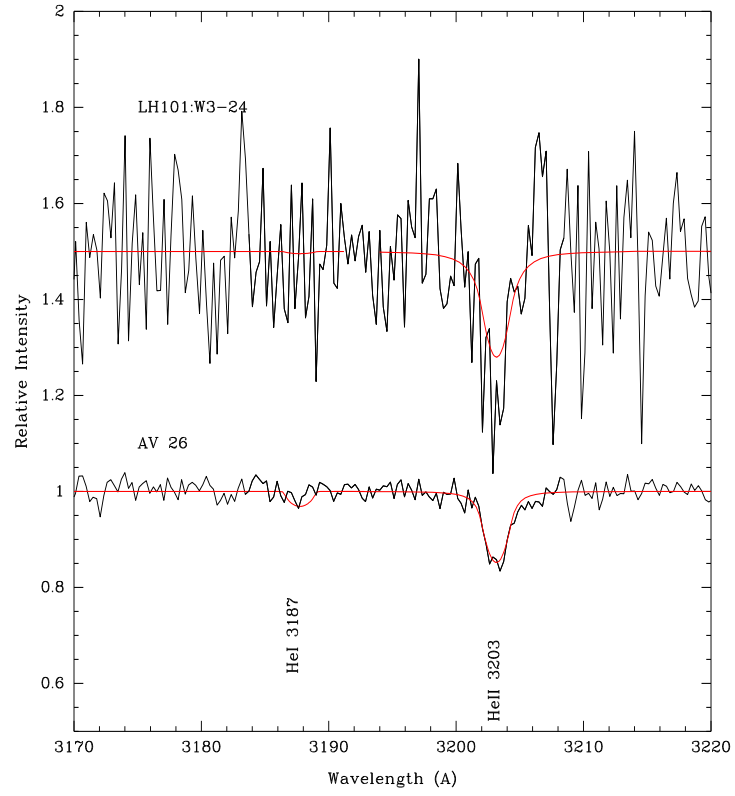
Fig. 24.— R136-055. The same as Fig. 19.

Fig. 25.— He Iλ3187 and He II λ3203. The near-UV region of the spectrum (black) is shown for AV 26 and LH101:W23-24, along with the model fits (red).
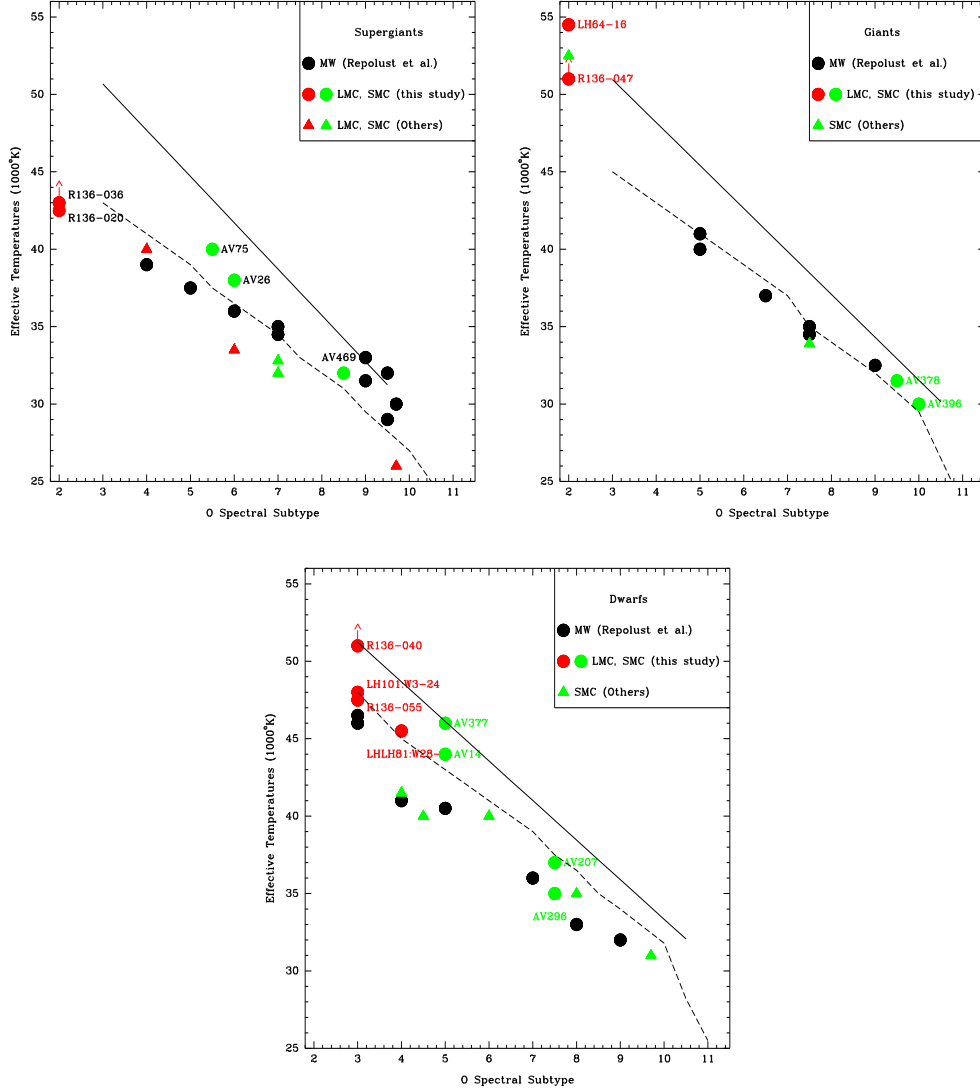
Fig. 26.— Effective temperature scale as a function of spectral subtype. The scale on the x-axis corresponds to the spectral subtype (2=O2, 5.5=O5.5, 10=B0, 11=B1) for the three luminosity classes. The black filled circles are the results of model fits to Galactic stars, taken from Repolust et al. (2004). The red (LMC) and green (SMC) filled circles are from the present study, while the red (LMC) and green (SMC) triangles are the results of CMFGEN modeling from Crowther et al. (2002), Hillier et al. (2003), and Bouret et al. (2003). The solid line corresponds to the effective temperature scale of Vacca et al. (1996), and the dashed line corresponds to the effective temperature scale of Conti (1988).